



**Australian Government**  
**Department of Defence**  
Defence Science and  
Technology Organisation

## A Record of the Australian Mirage Wing Fatigue Test

*R.A. Bruton and C.A. Patching*  
*Edited by*  
*R. Krieser and L. Molent*

**Air Vehicles Division**  
Platforms Sciences Laboratory

DSTO-TR-1561

### **ABSTRACT**

A full-scale fatigue test was completed in August 1974 on a Mirage III0 starboard wing utilising a loading spectrum as specified by the Royal Australian Air Force (RAAF). To satisfy a variety of RAAF missions, twelve (12) servo-hydraulic actuators situated at critical locations on the wing reproduced the measured flight strains. The fatigue loading flight-by-flight sequence was derived from fatigue meter data that was obtained from the Mirage fleet and from continuous records from an instrumented Mirage in the squadron service. The conduct and results of this innovative test are summarised here.

### **RELEASE LIMITATION**

*Approved for public release*

*Published by*

*DSTO Platforms Sciences Laboratory  
506 Lorimer St  
Fishermans Bend, Victoria 3207 Australia*

*Telephone: (03) 9626 7000*

*Fax: (03) 9626 7999*

*© Commonwealth of Australia 2004*

*AR-013-047*

*March 2004*

**APPROVED FOR PUBLIC RELEASE**

# A Record of the Australian Mirage Wing Fatigue Test

## Executive Summary

A successful full-scale fatigue test of a RAAF Mirage III0 starboard wing was completed at DSTO's Fisherman's Bend laboratory in August 1974. The wing was supported in a rig simulating the fuselage and the test load was applied by 12 servo controlled hydraulic jacks – 8 jacks applying upward forces to the wing, 2 applying downward forces and 2 applying the undercarriage reactions. The fuel tanks were also pressurised. This was DSTO's first multi-load channel full-scale fatigue test and the first which used a flight-by-flight spectrum derived from flight measurements. A formal report was not published at the time, though a draft existed and forms the basis of this current report. This report summarises, for historical reasons, the conduct and some significant results from this innovative (at the time) test program.

# Authors

## **R. Krieser**

Air Vehicles Division

*Mr. Krieser graduated in 1962 with a Diploma in Radio Engineering from the Royal Melbourne Institute of Technology. Since commencing employment at the then Aeronautical Research Laboratories in 1956, Mr Krieser has worked in the fields of Flight Instrumentation, Airborne Data Acquisition, Analogue flight simulation, Helicopter Fatigue Life Usage Instrumentation, and as the Finance Manager for the International Follow-On Structural Test Project (IFOSTP). (i.e. He was involved in the construction of the first ARL Analogue computer used for aerodynamic flight simulation, the data acquisition equipment for the ENTEC anti-tank missile, design and construction of airborne data acquisition hardware and the design and development of a Fatigue Life Usage Indicator (FLUI) for the RAN Wessex and Sea King helicopter fleet. The equipment was subsequently patented and adopted by Westland Helicopter Ltd (UK) as a standard transmission gearbox life usage monitoring hardware). He has been attached to the DSTO Business Office as a technical advisor and attended the Paris Air-show as the DSTO technical representative at the Australian Department of Trade stand. Ray was also seconded to the DSTO recruitment office as a selector of candidates for DSTO laboratories. Ray has recently retired after forty-six years of service at DSTO. He is currently employed on a contractual basis to assist the IFOSTP task manager at the Platforms Sciences Laboratory in the area of RAAF financial reporting.*

---

## **L. Molent**

Air Vehicles Division

*Mr. Molent graduated in 1983 with a Bachelor of Engineering (Aeronautical). Since commencing employment at the then Aeronautical Research Laboratories in 1984, Mr Molent has worked in the fields of aircraft structural integrity, aircraft fatigue monitoring, structural and fatigue testing, advanced bonded repair, aircraft accident investigation and aircraft vulnerability. He has over 100 publications in these technical areas. He has been attached to both the Civil Aviation Department (1985) and the US Navy (NAVAIR, 1990-1991) as an airworthiness engineer. Mr Molent completed a Graduate Certificate in Management in 1997. Mr Molent is currently a Senior Research Scientist and task manager of the F/A-18 Structural Integrity and manager of the International Follow-On Structural Test Project, at the Platforms Sciences Laboratory.*

---

# Contents

1. INTRODUCTION .....	1
2. PLANNING OF TEST.....	2
3. TEST SPECIMEN .....	5
3.1 Main Spar .....	6
3.2 Material specification - main spar .....	9
3.3 Pre-test inspection of wing .....	9
4. DERIVATION OF TEST LOADS .....	13
4.1 Flight loading and ground calibration.....	13
4.2 Analysis of flight tests .....	16
4.2.1 Statistical analysis of flight-data.....	16
4.2.2 Comparison of predicted data with measured data.....	17
4.3 Derivation of actual test loads.....	20
4.3.1 Theoretical load distribution.....	20
4.3.2 Fitment of fairings .....	20
4.3.3 Rejection of airbrakes loads .....	22
4.3.4 Simulation of elevon and supersonic tank loads .....	22
4.3.5 Method of generating resultant wing load distributions.....	23
4.3.6 Calculation of jack loads.....	27
5. LOAD SEQUENCE .....	30
5.1 Service conditions.....	30
5.2 Service data .....	30
5.3 Data reduction .....	30
5.4 Manoeuvre load cases .....	31
5.5 Representation of manoeuvre load sequences.....	32
5.6 Mission sequence.....	33
5.7 Truncation of load sequence.....	33
5.8 Ground load representation.....	34
5.9 Wing fuel tank pressurisation.....	34
5.10 Flight-by-flight load representation.....	36
5.11 Load sequence applied during test.....	36
6. CONTROL TAPE.....	38
6.1 Creation of control tape .....	38
6.2 Verification of control tape.....	40
7. DESIGN AND MANUFACTURE OF TEST RIG.....	40
7.1 Hydraulic actuator control system.....	42
8. TEST ARTICLE INSPECTIONS.....	42
9. DATA ACQUISITION .....	43
9.1 Static Strain Surveys .....	43
9.2 Continuous recorded strain data.....	43

<b>10. TEST ARTICLE FAILURES.....</b>	<b>44</b>
<b>10.1 Final failure.....</b>	<b>45</b>
<b>10.2 Cracks in lower rear flange bolt holes .....</b>	<b>47</b>
<b>11. CONCLUSION .....</b>	<b>47</b>
<b>12. ACKNOWLEDGEMENTS.....</b>	<b>47</b>
<b>13. REFERENCES.....</b>	<b>51</b>
<b>APPENDIX A: WING TRANSDUCER DESCRIPTION.....</b>	<b>57</b>
<b>APPENDIX B: DESIGN AND MANUFACTURE OF THE TEST RIG .....</b>	<b>59</b>
<b>APPENDIX C: ACTUATOR CONTROL SYSTEM (VALVE PACK) .....</b>	<b>71</b>
<b>APPENDIX D: SUMMARY OF CONCLUSIONS FROM THE MIRAGE SCATTER FACTOR FOR WING FATIGUE TEST MEETING.....</b>	<b>77</b>

## Abbreviations

AFTRAS	Airborne Flight Trial Analogue System
ARL	Aeronautical Research Laboratories
CAC	Commonwealth Aircraft Corporation
F+W	Swiss Federal Aircraft Factory
GAF	Government Aircraft Factory
GAMD	Generale Aeronautique Marcel Dassault
POF	Probability of Failure
PSL	Platforms Sciences Laboratory
RAAF	Royal Australian Air Force
V-g-H	A Velocity-normal acceleration-Height combination
WSRL	Weapon Systems Research Laboratory

# 1. Introduction

In 1965 the Mirage III0 aircraft (Figure 1) entered service with the RAAF as a tactical fighter. Changes in its Australian operational role to a ground-attack aircraft caused more severe fatigue loading on the aircraft than anticipated by the manufacturer. The aircraft was retired from RAAF service in 1984 and was replaced by the F/A-18.



Figure 1: A RAAF Mirage in Flight

Following a request from the RAAF to the (then) Aeronautical Research Laboratories (ARL)<sup>1</sup> to determine the safe-life of the aircraft under Australian operating conditions, a comprehensive flight test program was initiated in 1967. The aim was to determine the actual strains in critical areas of the structure at different altitudes and speed, and measure variations in temperature during certain missions. The results from the flight test program suggested that the main spar was the most fatigue critical component. A safe-life estimate was made on a single spar fatigue test. A load monitoring program was started by fitting a fatigue meter to each aircraft and registering the 'g' level exceedance counts thus enabling an accumulation of fatigue damage (by aircraft "tail" number) to be calculated. A safe life of 2,300 hours was determined, a figure well below the 4,000 hours required by the RAAF for its peace time training, thus necessitating the life of type to be established for the aircraft.

The manufacturer's spar test (Ref.1) was considered of limited value at the time because:-

- (a) as a major component test, it only simulated the load diffusion effects from the large lower fuel tank panels by incorporating "representative" narrow, but thick plates attached to the spar flanges;
- (b) the test loading was a simplified two level program, with one load considerably higher than the other;

---

<sup>1</sup> At the time part of the Department of Supply. Now DSTO Platforms Sciences Laboratory.

- (c) load application was concentrated at one span-wise point, ie., 1,285 mm from centre line of root attachment pins. This gave a stress distribution substantially different from the design and the values found in subsequent flight-tests.

To overcome the perceived inadequacies of spar fatigue test data, and insufficient data on flight load history relevant to the Australian operation of the Mirage, it was decided to conduct a full-scale fatigue test and conduct a comprehensive flight test program. To this end a high life wing was instrumented to provide the necessary data from which to derive the test loads, Refs 2 to 8, and the design of the test rig undertaken. A range of computer controlled flight loads applied by a unique servo-hydraulic loading system was devised to effectively use the derived data to simulate as closely as possible the in-service flight parameters.

While the wing, especially the first 455 mm of the main spar, were considered to be the major concern, other vital areas eg. fuselage frames 26 (main spar connection), 32 (rear spar connection), 33 (fin connection) and the fin spar were also considered to be fatigue critical. Strain investigations, together with more refined calculations were to proceed in collaboration with the Swiss Federal Aircraft Factory (F+W) which subsequently also conducted a fatigue test on a complete aircraft.

Approval for the fatigue test at ARL was eventually given by the Department of Air in August 1972, requesting a commencement in mid-January 1974 with a milestone of 9,000 test flights to be completed by August 1974. Some months later this time scale was reduced for a start in mid-December 1973 and 9,000 test flights to be completed by the end of April 1974.

The test started on 17<sup>th</sup> January 1974 and reached the 9,000-flight milestone on the 7<sup>th</sup> April, some 23 days ahead of schedule. The test was run on a continuous basis (with some interruptions due to malfunctions, inspections and repairs) until the wing spar failed unexpectedly on 20<sup>th</sup> October 1974, after 32,372 flights.

A paper was presented at the Eighth Symposium of the International Committee on Aircraft Fatigue (ICAF) (Ref.9) in 1975 describing the design of the test to simulate the wide range of service conditions and the preliminary results. This report contains an overall historic description of the numerous tasks undertaken before during and after the test, and references the supporting work done during the investigation.

## **2. Planning of Test**

Prior to the decision to fatigue test a complete wing, consideration was given to a number of proposals. These included a repetition of the manufacturer's (GAMD) spar fatigue test with improvements to the load distribution along the spar. Also considered was the fatigue testing of a wing with a single load distribution to include a representative load transfer into the spar flanges. A load sequence representing Australian service load conditions was to be applied.

After consideration of cost, complexity and time available, it was decided that flight conditions involving the variable load distribution that occurs in a tailless delta could be simulated in the laboratory. The advantages of conducting such a comprehensive fatigue test were considered at the time to be to:

- (a) make possible a reliable estimate of the safe life for the wing by reducing to a minimum the loading unknowns;
- (b) allow inspection procedures to be developed for use in service; and
- (c) provide data for the design of (and hopefully test) any necessary modifications.

Such a test was to be achieved by:

- including manoeuvre, gust, landing, taxiing and fuel tank pressurisation loads,
- using a test load sequence that would follow real flight-by-flight continuous service load histories,
- controlling the test with a computer commanding a closed-loop, servo-hydraulic loading system that varied the load distribution over the wing for each load turning point,
- using a test wing that was firstly instrumented, ground calibrated, and flown to provide in-flight data as a means of calibrating the rig, and thus assuring the degree of representation between the laboratory test loads and the loads experienced in flight,
- using a test wing that had seen sufficient service to possibly contain fretting and or corrosion effects.

The input data used to design and conduct the test came from a variety of sources and included the following:

- (i) Report on GAMD static strength tests containing deflection measurements and a finite element analysis for strain in the fuselage (Ref.10) which permitted the design of dummy fuselage.
- (ii) Various data relating to the applied loads and their sequencing including:-
  - GAMD design calculations for the aircraft,
  - Wind tunnel pressure plots for a clean aircraft from F+W, Switzerland, (Ref.11),
  - DSTO's (then) Weapons Systems Research Laboratory (WSRL)<sup>1</sup> and ARL aerodynamic data from wind tunnel tests on a 1/50<sup>th</sup> scale model giving resultant lift and moments at a variety of flight conditions, aircraft weight and stores configurations (Refs 12 and 13),
  - RAAF Aircraft Research and Development Unit and ARL flight strain data and gust velocity measurements (Figure 2) from an instrumented aircraft fitted with a gust probe (Figure 3), which also provided information on the elastic response of the aircraft (Ref.14),
  - Load histories for landing and take-off from the ARL test flight program,
  - Fatigue meter counts (g exceedances) together with frequency and sequence of service flight missions from fatigue meter sheets compiled by RAAF flying units,
  - Strain - load relationships and deflection information from ground calibrations made by ARL on the instrumented aircraft that were also used for processing flight strain data.
- (iii) A combination of flight measurements and ground calibrations (Ref.34), to give the basis for the direct calibration of the test rig by checking the correct transfer of flight loads into and along the spar to the root. This provided confirmation of the vital relative stiffness between spar root attachment lugs and dummy fuselage.



Figure 2: ARL Designed V-g-H Cassette Tape Recorder for Mirage Gust Load Studies



Figure 3: Gust Probe Mounted to Flight Trials Aircraft

The project manager (C.A. Patching) appointed to plan and control this fatigue test was advised on technical matters by a research and development committee whose main function was to derive test load conditions using the above data. Engineering support was provided by two then existing local aircraft firms; Commonwealth Aircraft Corporation (CAC) and Government Aircraft Factory (GAF), for the derivation of test load distributions, design and construction of the test frame, preparation of the test specimen and provision of technicians for running the actual test.

The project was divided into two stages, one involved with preparation for the test and the other with the actual testing. The initial assumption was that the test rig would be ready for commissioning by October 1972, with start of test by mid-January 1974. After planning had commenced, a revision was made to shorten the preparation stage by one month so that a test milestone of 9,000 test flights could be reached by the end of April 1974.

Minor delays and unforeseen problems encountered ranged from delays in the approval of funds for contractors, to difficulties in computer programs used in the analysis of flight data and the derivation of test loads.

The test started on the 17<sup>th</sup> January 1974. Initially the rig was run only during normal working hours. Later on shift running was introduced. During the initial period the rig was 'tuned' to obtain the optimum cycling rate, which involved changing of load cells on some channels to give improved response. Checks on calibration, load repeatability and accuracy were also made during this period.

At the start of the testing stage, an operating schedule (Figure 4) was planned to ensure the 'milestone' of 9,000 flights would be reached by the end of April 1974, followed by a further goal of 15,000 flights by August 1974. The assumptions were:

- A one shift operation until 6 February 1974, then three shifts, seven days a week until final failure,
- Three types of inspections would be conducted namely;
- type 'A', visual every 250 flights taking 3 hours;
- type 'B', wing removal every 750 flights, 40 hours down time; and
- type 'C', radiographic inspection of critical areas every 2,250 flights, in conjunction with wing removal, taking 120 hours.
- A cycling rate of 9 cycles per minute (cpm) (i.e. 75% of design rate of 12 cpm).

These assumptions gave a 26.5 day testing period between 'C' inspections (i.e. 2,250 flights including two 'B' inspections and six 'A' inspections).

Figure 4 shows:

- planned schedule together with what was achieved,
- a table listing the test flights when inspections were done,
- the Rig Operational Efficiency calculated on a cycling rate of 20 cpm (which was the average loading rate achieved after the test had settled down to a tuned and routine running procedure),
- a 24 hour day with no scheduled or un-scheduled stoppages.

The highest overall running efficiency was 44% (up to 15,455 flights) when the rig was stopped for 61 days due to the first wing failure.

For the purpose of reporting this investigation, the tasks in the original planning schedule were arranged as shown in Figure 5.

### 3. Test Specimen

Despite the known limitations arising through not testing a full span wing mounted on a fuselage, there were two compelling reasons which resulted in one wing only being tested. These were, the time and cost required to create the loading rig, and secondly, the RAAF had only one wing in excess of their operational requirements.

The test article selected was a starboard wing, serial no. R 41UK/No 10 (CAC/10), which later transpired<sup>2</sup> to be the last RAAF Mirage wing to have been fully assembled in France (Figure 6). It had flown 1,792 hours on RAAF Mirage A3-10 before removal and being instrumented for the test flying on Mirage A3-76. Since the test life was to be related to the average of the 1972 Australian service flight-loading spectrum, the prior equivalent fatigue test life of this wing reduced to 1,142 hours.

The Mirage wing, of delta plan-form, had a span of 3.3 metres with a root chord of 6.3 metres and contained three spars; front, rear and main spar. Figure 7 shows the lower surface and plan-form of the test wing and the areas occupied by the undercarriage and dive brake forward of the main spar. The large integral fuel tanks were bounded by the root rib, main spar, front and rear spars. This integral tank formed the torsion box of the wing. Figure 8 indicates the Mirage III lower surface showing positions of wing spars and the location of test instrumentation. Details of the wing transducers are provide in Appendix A.

### 3.1 Main Spar

While the wing contained three spars, the main spar was the major structural member designed to react to bending, shear, and a portion of the torque and drag loads.

Figure 9 shows the aft side of this spar. The end lug were well proportioned to alleviate the stress concentration around the attachment pinholes. Another feature of the spar was the heavy section diagonal bracing of the shear web to resist bending and torque loads inboard of the root rib. The large hole housing the main undercarriage trunnion bearing is also shown in this figure.

A further aspect of the main spar design was the exposure of a strip of the lower and upper boom flanges to the heat generated in the aerodynamic boundary layer at supersonic speed. The inboard section of this exposed strip, situated between the forward and aft lower flanges of the main spar (which minimised any thermal gradients and hence stresses in the booms), is shown in Figure 10.

---

<sup>2</sup> This was not discovered until the cracking of anchor nut rivet holes became an issue in the RAAF fleet. In France these holes were jig-drilled, while at CAC they were produced by hand, leading to a significant variation in edge distance. Thus cracking occurred in some wings in the RAAF fleet but not this test article. Boron epoxy doublers were fitted to RAAF aircraft to address this problem (see Ref 35).

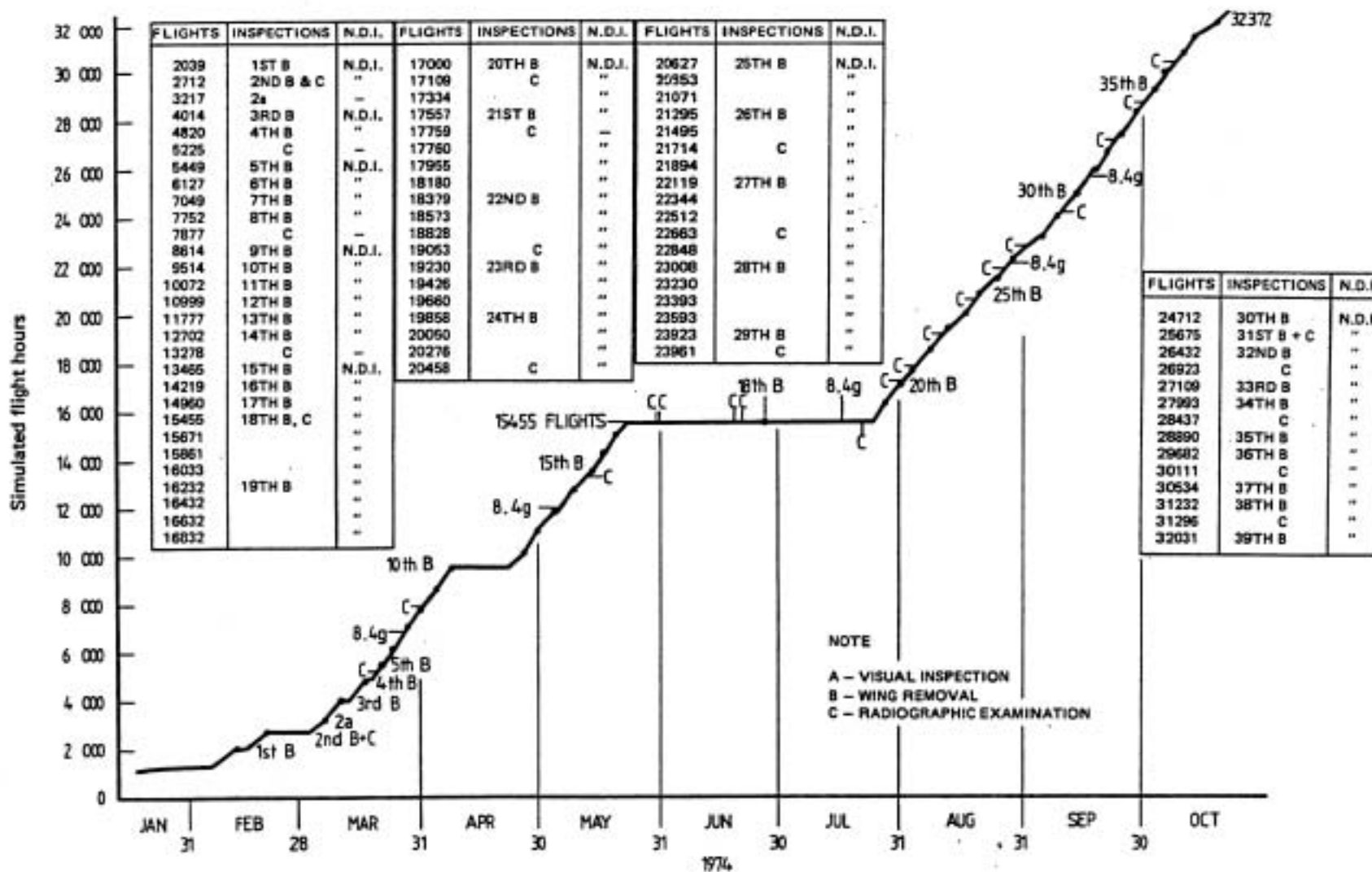


Figure 4: Mirage Wing Fatigue Test Operating Schedule

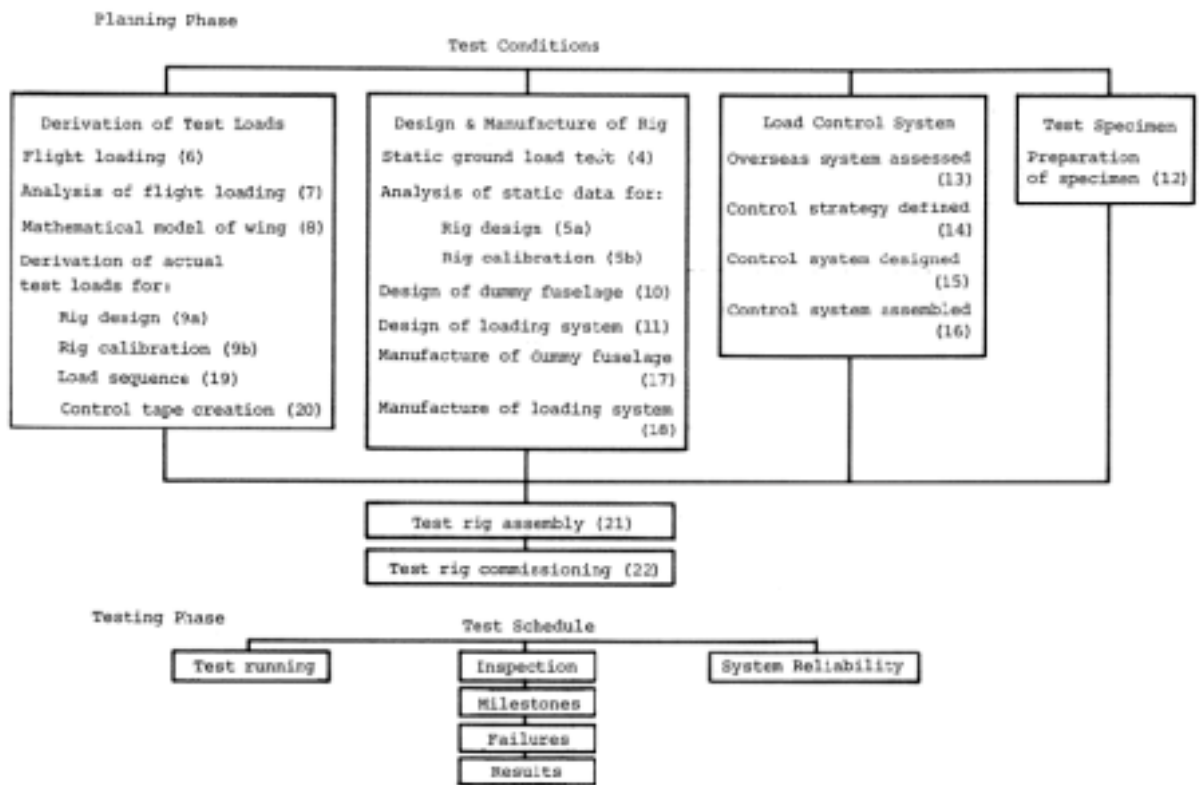
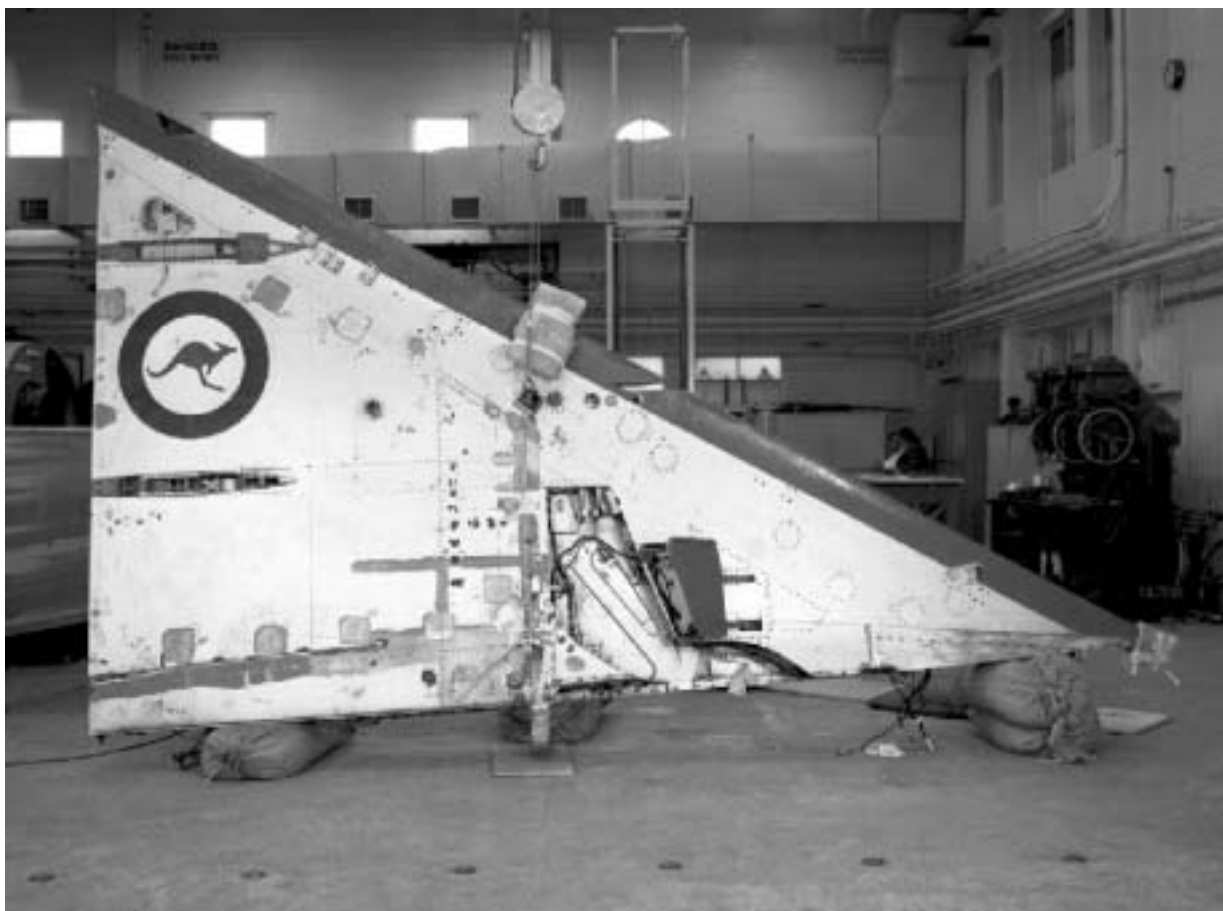


Figure 5: Fatigue Test Tasks



*Figure 6: Lower Surface of Test Wing*

### **3.2 Material specification – main spar**

The aluminium alloy used in construction of the forged main spars was A-U4SG (U.K. and U.S.A. equivalents are 2L65 and 2014S respectively). Following the fatigue test, specimens were cut from the main spar and the material composition was found to be close to the nominal A-U4SG specification. The mechanical strength properties were found to exceed specification requirements.

### **3.3 Pre-test inspection of wing**

The wing was inspected at CAC prior to fatigue testing [Ref.16] to:

- ensure that the wing was in a serviceable condition.
- establish the modification status of the test wing.
- establish the condition of the wing prior to testing ie. the presence of any fatigue cracks or corrosion.

The report declared the wing to be within mensuration tolerances and fully serviceable.

The following CAC modifications had been incorporated: No.s 27, 78, 118, 128, 288, 313, 376, 399, 416 and 595.

Cracks were found at several rivet holes in the skin above the wheel-well. Those cracks had been found in most service aircraft.

It was decided to commence testing with the cracks present in order to obtain data on rates of crack growth and incorporate a repair along with the GAF modification No. 761 some time later. The skin replacement repair was done at 9,514 flights as reported in Ref.15.

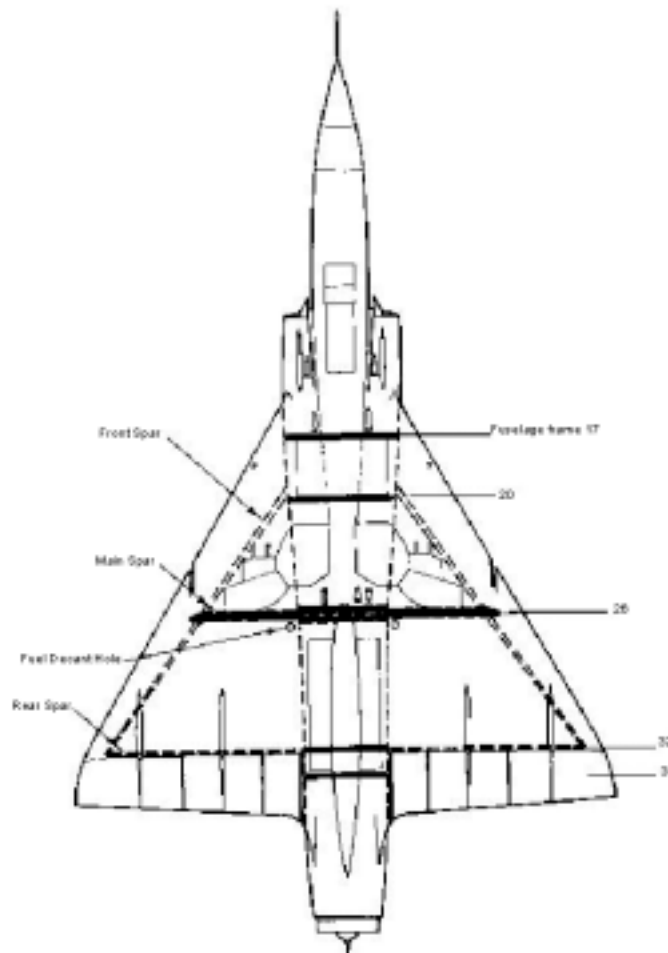
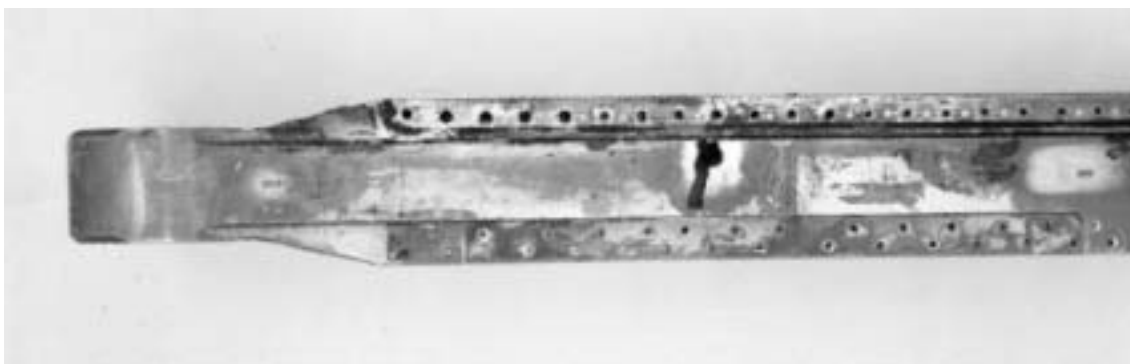


Figure 7: Mirage III Lower Surface Showing Positions of Wing Spars





*Figure 9: Aft Side of Starboard Main Spar Showing Diagonal Brace*



*Figure 10: Inboard Section of Main Spar Showing Exposed Central Strip between Fore and Aft Lower Flanges*

## 4. Derivation of Test Loads

To derive the magnitude and distribution of the aerodynamic loads on the actual test wing accurately, a flight test program was conducted.

The initial flight tests (stages 1 and 2) had been started in 1967. They were undertaken to gather data in order to improve the life estimation calculations. These tests included high and low altitude flights at various speeds, including fuselage data recording of typical RAAF squadron operations. Strains were measured at various stations along the main spar, upper and lower wing skin surfaces, frame 26, the nose and main undercarriages.

### 4.1 Flight loading and ground calibration

Following the 1973 decision to conduct a full-scale fatigue test on a wing, a further series of flight tests was made using the instrumented test wing to obtain:

- (a) load-strain relationships at the wing-to-fuselage attachments to assist in the design of the dummy fuselage;
- (b) load-strain distributions in both span-wise and chord-wise directions of numerous positions in the wing;
- (c) load-stress relationships in predicted critical areas for the derivation and adjustment of the test rig loads, and
- (d) data for use in a mathematical model of the wing structure.

A ground calibration was also conducted (Refs 17 and 34) on the test wing before flight-testing was started (Figure 11). The results:

- confirmed the functioning of all gauges and transducers.
- supplied experimental values for the static structural stress distribution.
- Determined strain-load relations that would permit flight load distributions to be estimated from measured flight strains.
- Obtained data that would indicate how the fuselage performance affected wing stresses.
- Allowed the effect of the wing to fuselage fairings on wing stresses to be evaluated.
- Obtained data for use in refining the mathematical structural model of the wing.

On-board data were collected using the DSTO developed Airborne Flight Trial Analogue System (AFTRAS), Figure 12 and Figure 13. The flight test data and analysis of the results were the basis for the derivation of the fatigue test loads [as stated in (c) above]. The data obtained from squadron usage of the aircraft were essential in the design of the laboratory fatigue test program.



*Figure 11: Test Aircraft Ground Calibration*

The analysis of the flight data was greatly assisted by the use and continual refinement of the structural mathematical model. This model was used to predict and trend-monitor the flight strains and through conversion of these strains into stress distributions allowed for the derivation of test loads. The model was also used to reduce the large number of combinations of type of flying missions and aircraft weight configurations (weight distribution) to a manageable number that represent the (then) current RAAF usage.

The results of this work are reported in Ref.18 with a description of the work given in Ref.11, including sample results and explanations for any discrepancies caused by the grid size and simplified assumptions as used in the model. In general the measured and predicted strains and deflections were compatible (ie. within +/- 15%). Initial analyses are presented in Ref.19.

The test wing was instrumented at 27 stations utilising over 83 strain gauges. These strain gauge positions were chosen to meet the requirements as outlined above. Figure 8 gives the description, layout, position and coordinates of each strain gauge. Also listed are five stations on the main undercarriage leg.

Selected RAAF pilots flew the test wing aircraft in conditions close to normal and average squadron operations. Data were recorded on magnetic tape and processed using the ARL PDP10 computer.

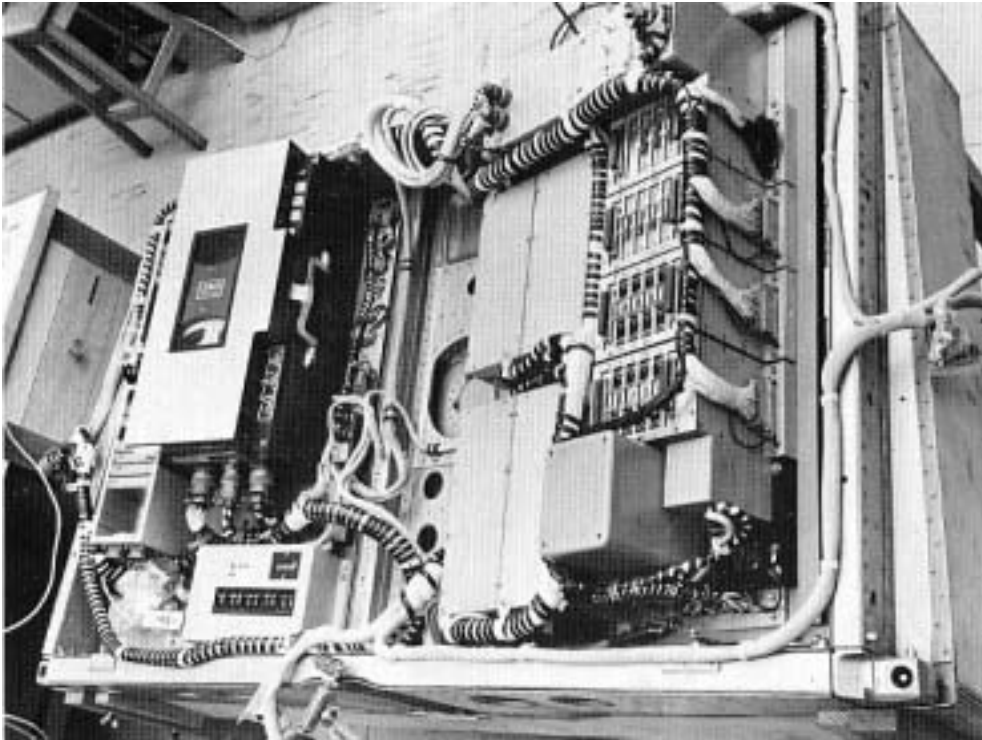


*Figure 12: The Mirage AFTRAS Unit shown in the Laboratory*



*Figure 13: AFDRAS Recorder in Rear Bay of Mirage*

The main problem encountered at the time was the handling and recording of such large quantities of data. Errors in the data and an instrument problem of cross channel coupling due to negative slew rate limitations, were not found until too late to be rectified.

### 4.2 Analysis of flight tests

The test wing was gauged and flown to obtain flight strain data that would lead to resultant wing loads and effective points of application. To assist in the analysis of the flight strain data in relation to the various types of loading experienced by the wing during each manoeuvre, a set of 15 parameters (Table 1) were recorded simultaneously. Flight load – strain relationships were then derived from analysis of flight strains and pre-flight ground load calibration strains.

Table 1: Flight parameters measured in flight test

Flight parameter	Recording speed
Forward acceleration	High
Lateral acceleration	High
Vertical acceleration	High
Pitch rate	High
Yaw rate	High
Heading angle	High
Bank angle	High
Pitch angle	High
Rudder position	High
Inboard starboard elevon position	High
Inboard port elevon position	High
True air speed	Low
Pressure altitude	Low
Mach number	Low

#### 4.2.1 Statistical analysis of flight-data

To obtain flight loads from flight-strains, a unique relationship between externally applied loads and measured strains had to be assumed. This requirement could not always be met because there were other factors influencing the strain being measured (eg. structural internal strains from thermal effect, errors in strain reading, hysteresis within the structure and position of the gauges relative to the externally applied load).

These problems can be overcome if the load-strain relationship is considered to be unique but statistical in value. If sufficient samples of load versus strain response can be taken, this unique relation can be estimated with minimal error.

A procedure was adopted that:

- Selected various gauge positions and types of gauges that would respond to one kind of load only, eg. (shear, torque, or bending moment). The gauges were located to yield information for purposes other than external load measurement so that some compromise was necessary.
- Conduct a series of ground load calibrations to establish:
- a sufficient sample of load versus strain data to permit statistical analysis to yielded load versus strain relations with reasonable mathematical accuracy,
- secondly, to automatically include this sample data in the evaluation of structural effects such as hysteresis and load position dependence,
- and thirdly, provide strain data for use in the refinement of a mathematical model of the wing.

The flight and ground calibration data were analysed using a statistical method (a multiple linear regression analysis) which provided the relationship between a set of variables for the purpose of prediction, estimation, and smoothing of data. To obtain a reliable result, the ratio of the number of readings to variables was set at 5 to 1.

The zero load condition was essential in solving the problem of combining the output of a number of strain gauge results. Zero external load did not necessarily correspond to zero strain because of internal loads, fuel pressurisation, thermal imbalance, weight of fuel, stores and loading introduced by the undercarriage.

The method used was to measure the bridge output under known loading conditions eg. (aircraft on ground), and its configuration and weight were measured precisely. From experimental load-strain relationship, the strain increment for each gauge was determined and the reading adjusted back to zero external load condition. This work was reported in detail in Ref.20.

#### 4.2.2 Comparison of predicted data with measured data

Preliminary estimates of load distribution had been made graphically for the purpose of planning, costing, and rig design. These early estimates were confirmed by comparing predicted with measured strain data prior to commencing rig manufacture.

To assist in the verification of the flight strain data, the port wing on the flight aircraft was strain gauged also but to a lesser extent.

The new flight data were converted into strain units using ARL developed software and together with the flight parameter data, were used to generate plots of continuous flight strain versus normal acceleration (Figure 14). Likewise, the flight data were analysed to give "instantaneous" values of strain by averaging very short time intervals of record.

Further processing of the flight data was done (Refs 20 and 34) to estimate wing net shear, torque about main spar, bending moment about root rib, loads in the leading edge attachment fitting, front spar upper and lower lug, and rear spar attachment fitting.

This analysis was done to give a sound basis for two methods of comparison, one between measured and predicted strain and the other using load as the comparison criteria.

This first comparison used flight strains that were predicted by applying theoretical loads to a computer structural model of the wing. The theoretical loads were obtained from software which simulated the aerodynamic and inertia load distributions of the aircraft for any flight conditions. The strains predicted by the wing structural model were scaled by "calibration constants" obtained for the aircraft flight conditions by comparing strains measured in a series of pre-flight ground calibrations and strains predicted under the same loading simulated on the computer model.

A plot of the predicted strains for positions along the main spar and those obtained by the averaging process of flight data, is shown in Figure 14. The strains in this figure were plotted versus NW eg. (acceleration x aircraft weight). This was done to allow comparison of various points in the flight. Similar comparisons were made for front and rear spars.

For the second comparison, two independent processes (to that described above) were used to obtain loads in the wing main load carrying members, using the flight strain measurements. The first was to estimate the overall wing resultant loads (using load strain correlations) obtained from an analysis of measured strain responses of the wing when subjected to a series of point loads during calibration ground tests. The derivation of the load-strain equations was described in Ref.20, and was based on methods developed by the National Advisory Committee for Aeronautics (NACA), Ref.21, and the Aeronautical Research Council (ARC), Ref.22.

The second process used loads at the wing to fuselage attachment points that were estimated from analysis of experimental strain-pickup-load relations obtained from ground calibration tests Ref.34.

Figure 15 shows the wing root bending moment predictions (by the former process), to be in good correlation with flight test estimations. This figure also shows the bending moment predictions for various Mach number and altitude combinations.

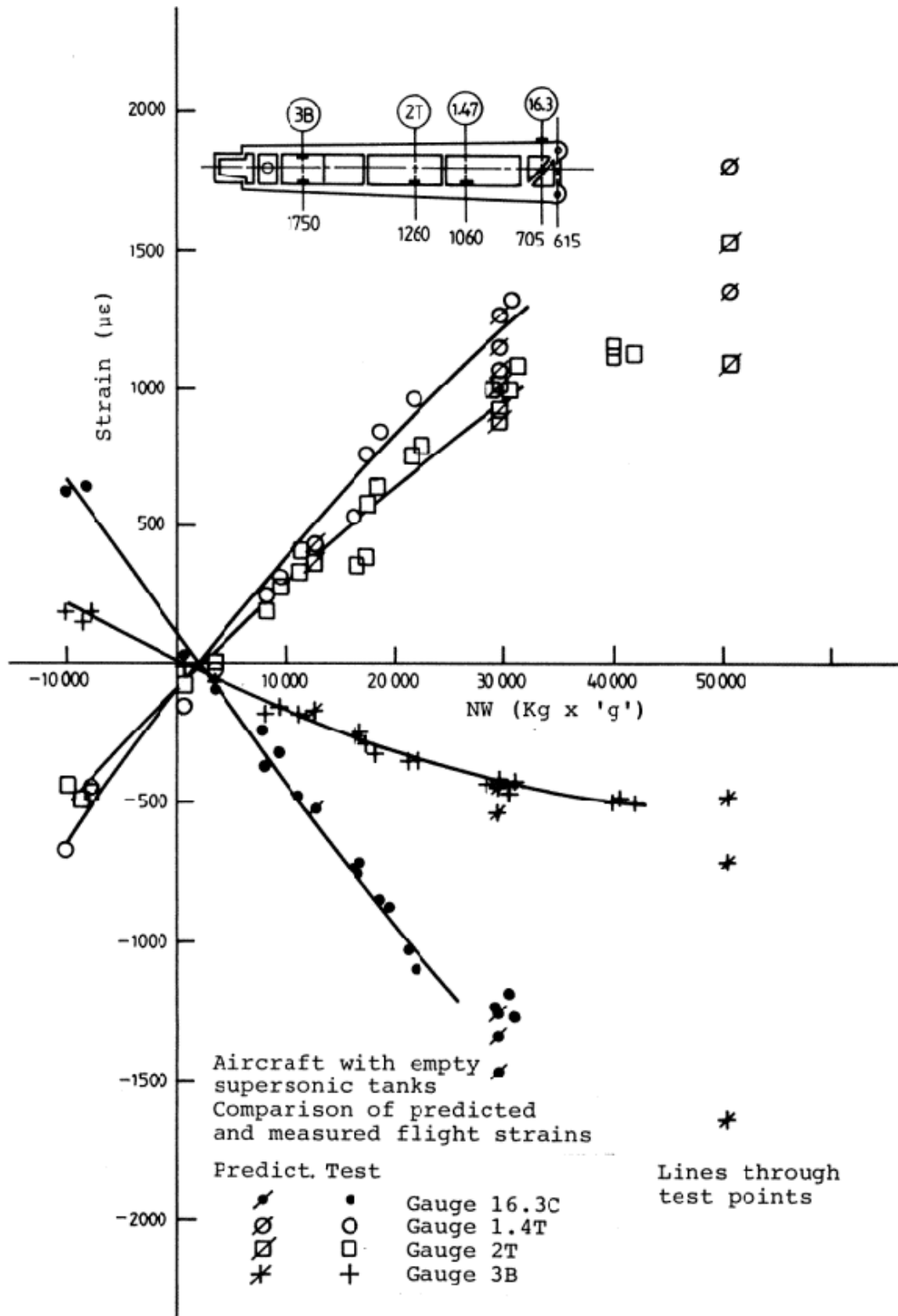


Figure 14: Comparison of Predicted and Measured Strains along the Main Spar

As can be seen from this work, good agreement was shown from comparisons of flight strain with predicted strain (using a structural model of the wing), and comparisons between wing loads, (derived from flight strain) and relevant flight parameters. There was however, some concern expressed at the time regarding “poor agreement” between predicted strains and those measured on the wing in the test rig at the front and rear spar attachment points (Figure 14). Similarly at points considered fatigue critical in the rear spar attachment points. This “difference” could have been caused by an inadequate representation in either the theoretical load distribution (applied to the structural model) or in the limitations of the mathematical assumptions of the model. Details of this work are reported in Ref.23.

### **4.3 Derivation of actual test loads**

When the analysis of test conditions was made, there was sufficient design and wind tunnel data available to know the range of test loads that would have to be simulated in the fatigue test. However, it was necessary to separate the task of test load derivation into its two essential parts, ie. That part concerned with rig design (Section 7), which only required the distribution and magnitude of maximum loads, and the other part that determined the actual fatigue loads and their sequence to be applied on test.

As the task proceeded and more data became available, the method used to derive the test loads was further enhanced to meet specific needs.

#### **4.3.1 Theoretical load distribution**

The first task was to produce a theoretical load distribution for the purpose of planning, initial rig design, costing and revealing any discrepancies in the available data Ref.24. For this work five flight-load cases were specified while use was made of the GAMD design office calculations and wind tunnel results including results from Swiss F&W wind tunnel tests.

#### **4.3.2 Fitment of fairings**

Early flight test results revealed some discrepancy in measured strain between gauges on the main spar and on fuselage frame 26. One explanation for this difference (approximately 10%) was the possibility that the fairings were providing an alternative load path. While the five pieces of fairings were relatively thin strips of aluminium alloy, those for the lower skin were flat and long with sufficient cross-sectional area to have significant load carrying capacity. A small percentage of load shedding was estimated to cause change in fatigue life. Therefore an investigation was conducted to determine the necessity of fitting fairings to the test wing. Fairings were obtained and gauged. Ground calibration tests were conducted with and without fairings fitted to provide an indication of:-

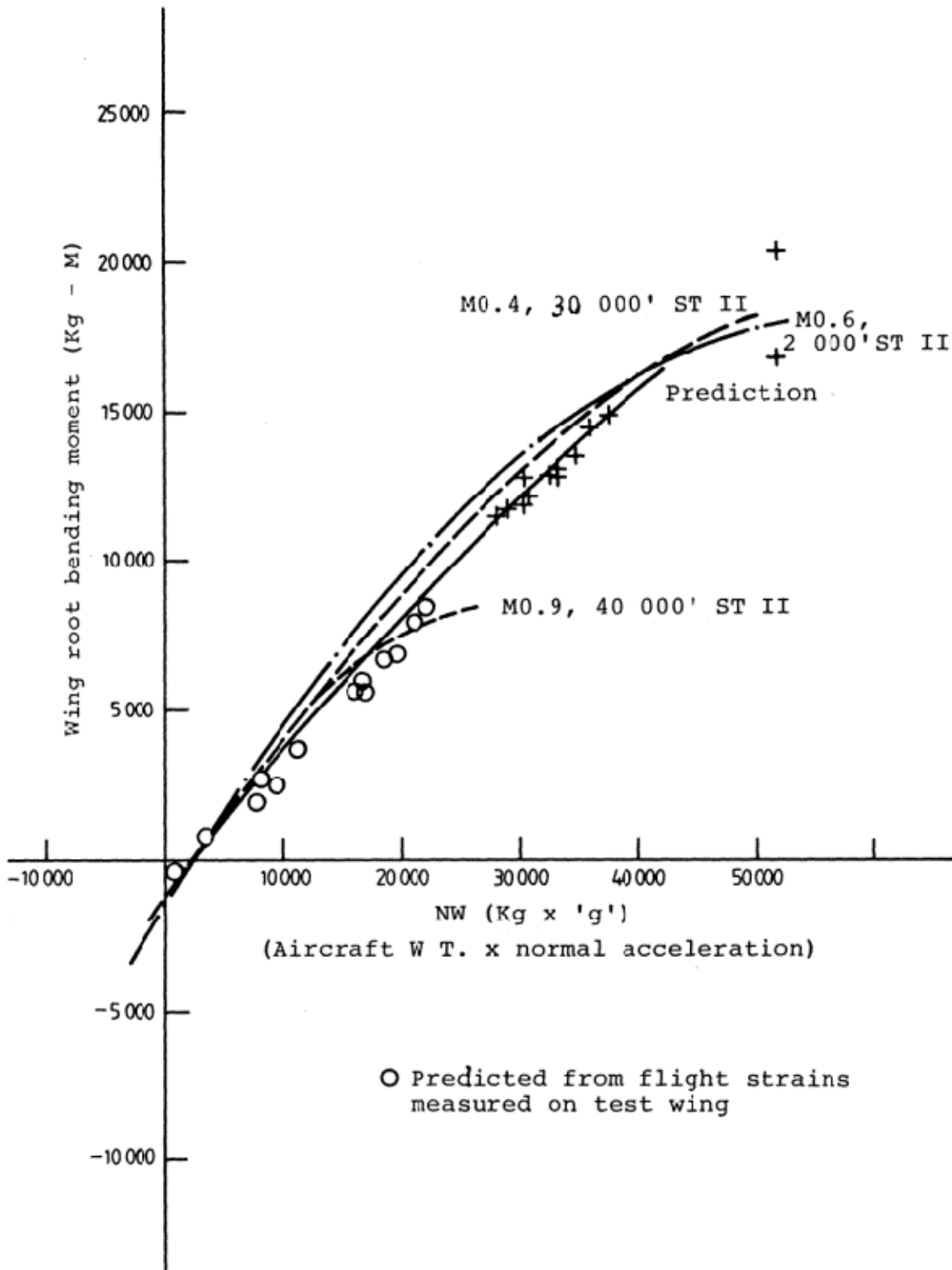


Figure 15: Wing Root Bending Moment Predictions

- the magnitude of loads being transmitted by fairings,
- which parts of the fairings transmitted significant loads.

The investigation, (Refs 25 and 26) showed that the fairings could carry up to 10% of the wing-bending load. Thus it was decided to fit fairings to the test wing.

#### 4.3.3 Rejection of airbrakes loads

An investigation (Ref.27) was conducted to determine if airbrake loads should be included in the fatigue test. Such loads were frequently used to affect some manoeuvres.

Air brakes not only introduced drag loads into the structure but also altered the lift-distribution in their vicinity and hence would affect bending moment and torque. Both these effects were analysed using GAMD data to obtain the drag coefficient for the six prescribed loading cases. Swiss wind tunnel data were used to investigate the changes in load distribution when the air brakes were extended.

This investigation showed that the structure in the immediate vicinity of the brake (ie. the rib attachments which support the unit to the front spar), could be affected. However, since this area was not a primary structure, theoretical fatigue lives would suffice for both the brake and its support structure.

The most significant effect of the airbrake operation as indicated by the structural model, was to increase the spanwise load experienced by the front and rear spar attachment points – a direction not considered during their design. However, an estimate of their ultimate strength showed that both fittings had more than adequate reserve strength margins in the spanwise direction. Therefore it was recommended that airbrake loads need not be simulated in the fatigue test.

#### 4.3.4 Simulation of elevon and supersonic tank loads

A further set of calculations (Ref.27) concerning elevon and supersonic tank loads, utilised additional wind tunnel data (Ref.11), which was obtained from a 1/50<sup>th</sup> scale model of Mirage IIIIO at WSRL for various stores, weapons configuration and a range of speeds (including supersonic flight). One aircraft configuration only was considered for these calculations; the one most frequently flown in service (empty supersonic tanks, half-total fuel at 50% wing centre-line chord, and a total aircraft mass of 8,403kg). Six flight-load conditions were considered embracing heights from 2,000 ft to 30,000 ft, Mach number 0.36 to 1.14 and load factors from 1.5g to 6g.

#### 4.3.5 Method of generating resultant wing load distributions

Eighty-one concentrated loads acting at nodal points on the wing (Figure 16), represented the wing load distribution for any load cycle turning point. The resultant wing load distribution for any load turning point was considered as being made up of three superimposed load distributions:

1. Air-loads caused by aircraft angle of attack;
2. Air-loads caused by the wing elevon angle; and
3. Inertia loads caused by wing mass, wing fuel and under-wing stores for normal aircraft acceleration.

The magnitude of total load (for each distribution point) at every turning point for manoeuvre, gust and landing load cases, was obtained from aircraft mass and dynamic balance calculations. This was achieved by scaling standard distributions up to the total load value required.

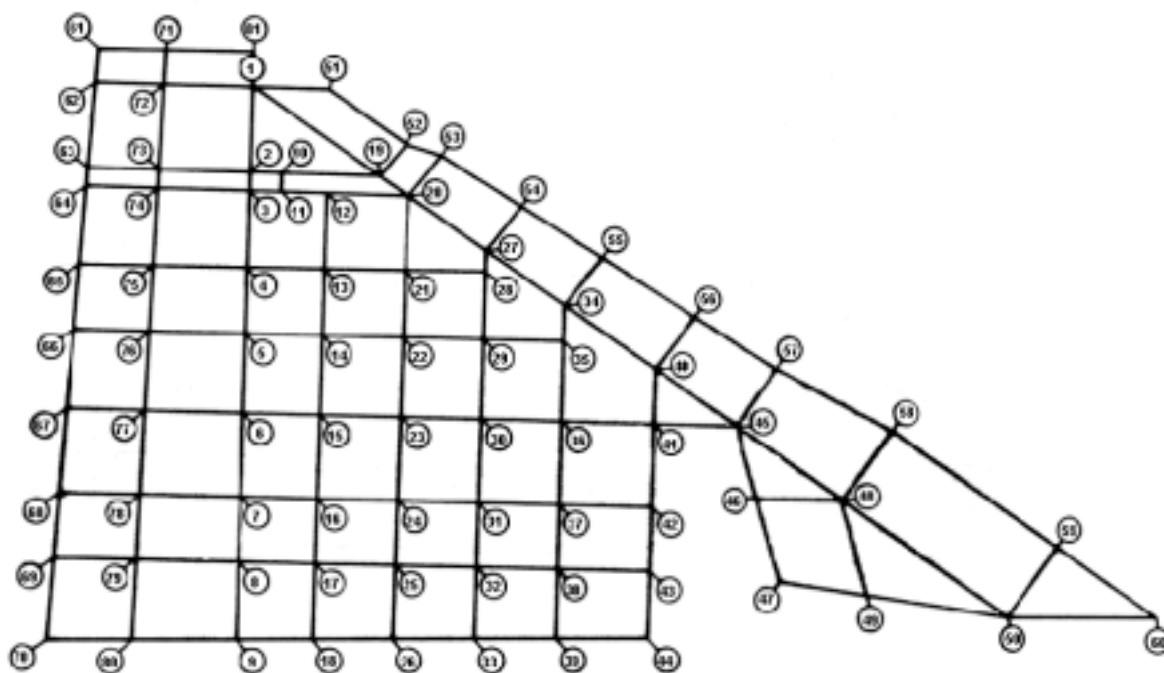


Figure 16: Nodal Point Representation of Wing and Elevon

This process was found to be the most convenient way of generating wing loads and derive a computer model of the aircraft wing load parameters. This was achieved by linking five separate models:-

1. A mass distribution model that calculated the aircraft weight and centre of gravity position for any wing mass distribution.

2. An aircraft dynamic balance model which calculated the total lift on the wing resulting from:
  - (i) angle of attack
  - (ii) elevon deflection for known aircraft weight,
  - (iii) centre of gravity position,
  - (iv) configuration (ie. fuel, stores, etc.),
  - (v) Mach number,
  - (vi) acceleration (both normal and pitch).
3. A wing load distribution model that determined how each of the three total loads generated by angle of attack, elevon and inertia were distributed; and estimated the resultant wing load distribution.
4. A gust load distribution model which derived resultant wing loads for the special conditions in a gust.
5. A landing load distribution model which generated the wing loads to be maintained when undercarriage loads were applied.

Figure 17 outlines the resultant combination of ARL input data and the five load parameter models. The figure shows that once the type-of-flying was known (whether it be gust, landing or manoeuvre load case), the resultant wing load distribution for the 81 nodal points could be calculated for each load cycle turning point. Details of the final distribution models are provided in Ref.28.

The resultant wing load distribution to be applied for a manoeuvre load case was the sum of the first three distribution models.

For the gust load case, two distributions were combined. Flight tests had shown that the strains in various parts of the wing, when flown through turbulence, were higher than those for manoeuvre loads producing the same normal acceleration. This was attributed to the fact that the frequency of gust loads was close to the primary wing bending mode frequency. The implication being that the wing load distribution from gusts was quite different from that caused by manoeuvre loads. As gust loads were estimated to cause significantly less fatigue damage than manoeuvre loads under typical RAAF operating conditions, it was decided to represent gust loadings in the fatigue test by those aircraft loads having the most commonly flown configuration. This configuration was an aircraft fitted with supersonic tanks, guns and practice bombs, half-the total fuel weight remaining, and flying at Mach number 0.7 at 2,000 ft with an all-up-weight of 8,970kg.

It was assumed that the resultant load distribution applied during the gust sequence, could be represented by the algebraic sum of a level flight distribution, and one representing the dynamic response of the aircraft to the gust disturbance factored by 'g'. The level flight distribution was derived from the above configuration (Figure 18).

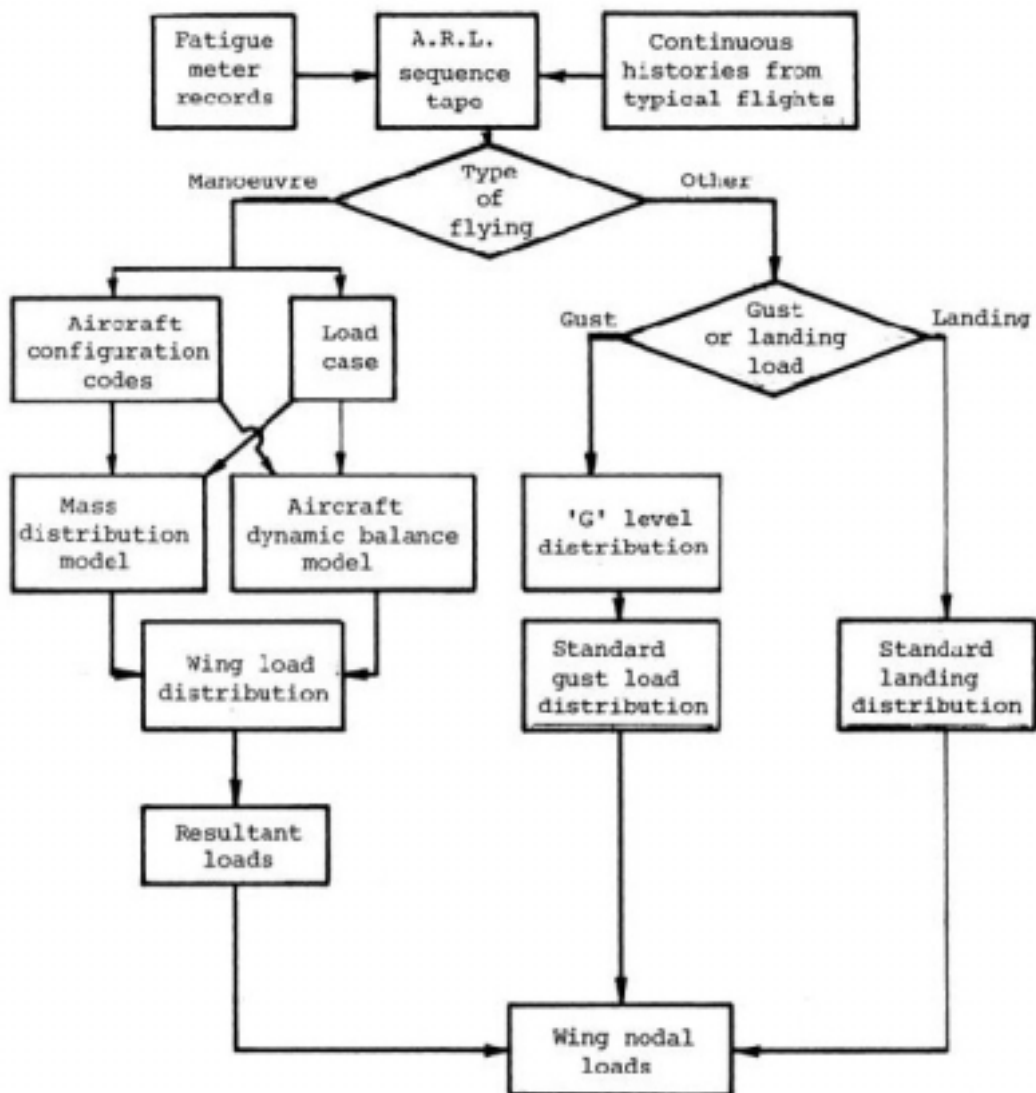


Figure 17: Calculation of Wing Load Distribution from Flight Parameters

The estimated distribution per 'g' used to represent the dynamic response of the aircraft is shown in Figure 19.

Only one load distribution was applied to the wing during the application of landing and taxiing loads. This distribution (Figure 20), represented the loading for an aircraft carrying supersonic tanks and guns with an all-up-weight of 7,793kg. The landing speed was measured in knots (Mach number 0.24), and altitude at zero (sea level).

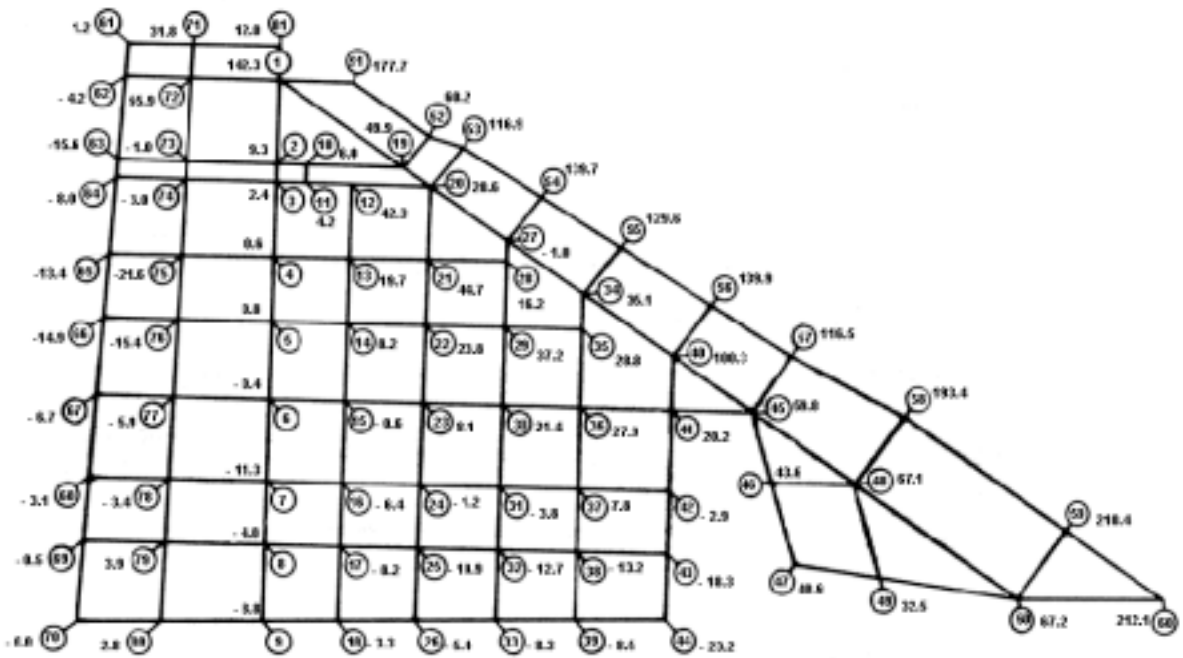


Figure 18: Level Flight Load Distribution (1g) Used as a base for Gust Loads (kg)

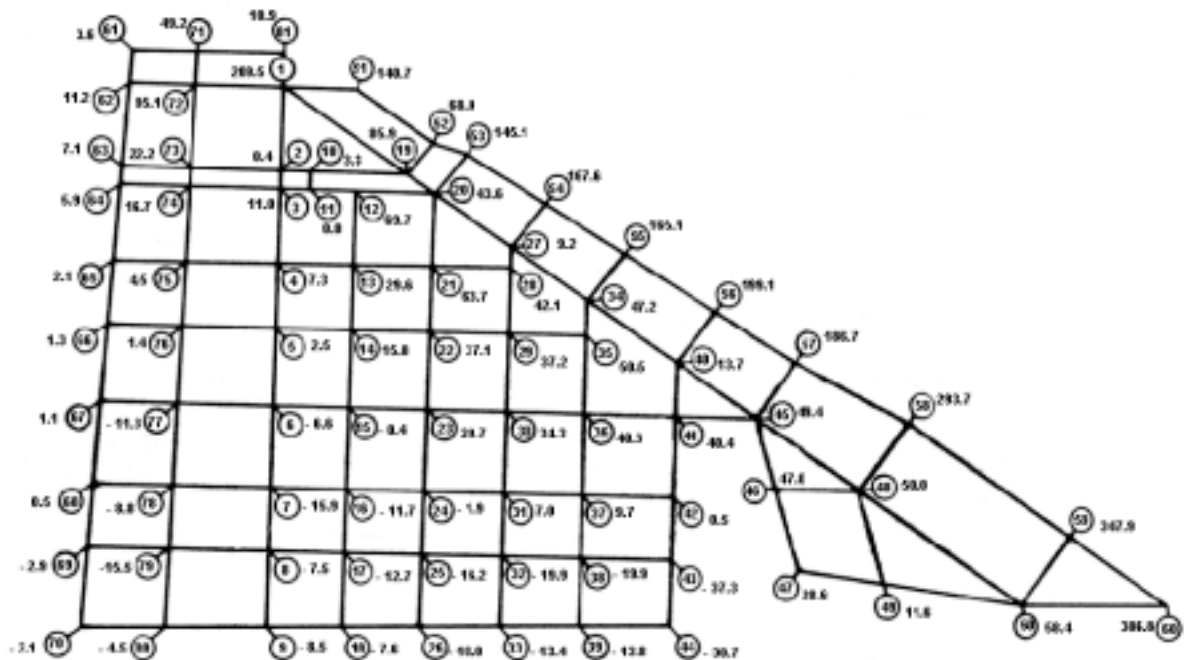


Figure 19: Estimated Distribution of Load per g due to Gusts (kg)

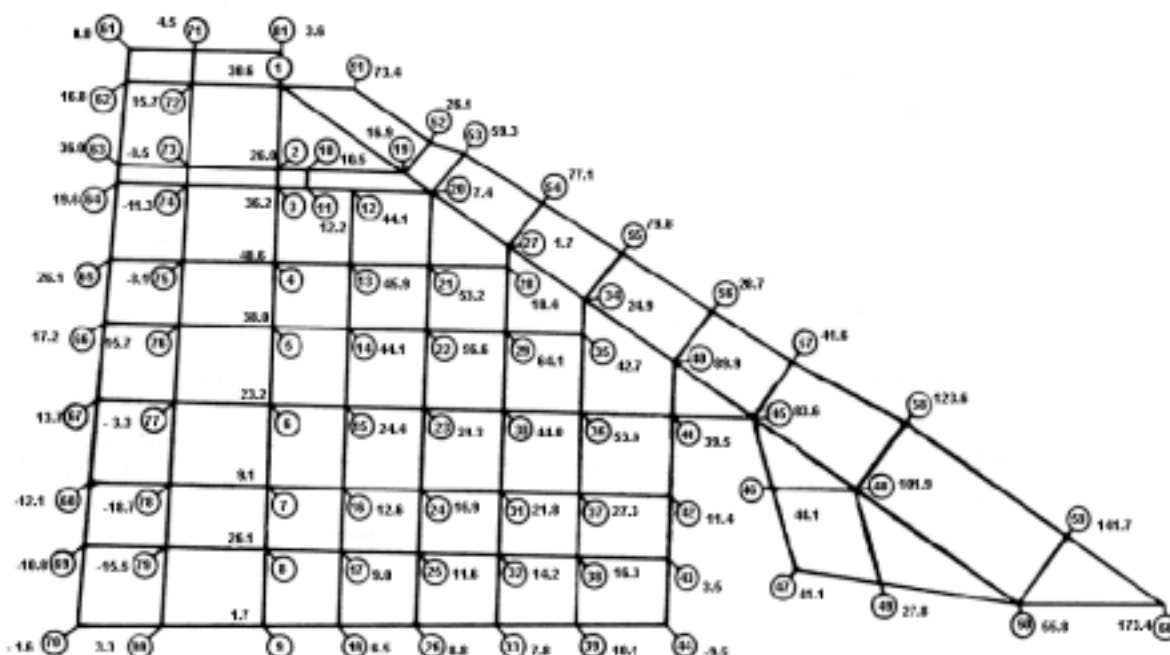


Figure 20: Load Distribution to Represent Wing Loads during Loading

#### 4.3.6 Calculation of jack loads

A process was derived to calculate the load distribution for each turning point in the test load sequence. The software program used incorporated input data that described the weight configuration (fuel, stores and type-of-flying mission) and the load distribution for each turning point in the test load sequence. The 81 nodal points were arranged in groups for connection to individual loading jacks. This was necessary for the rig design as it gave the capacity of each jack, its reaction position in the loading frame and secondly, for the data memory of the computer software to be used by the load control tape.

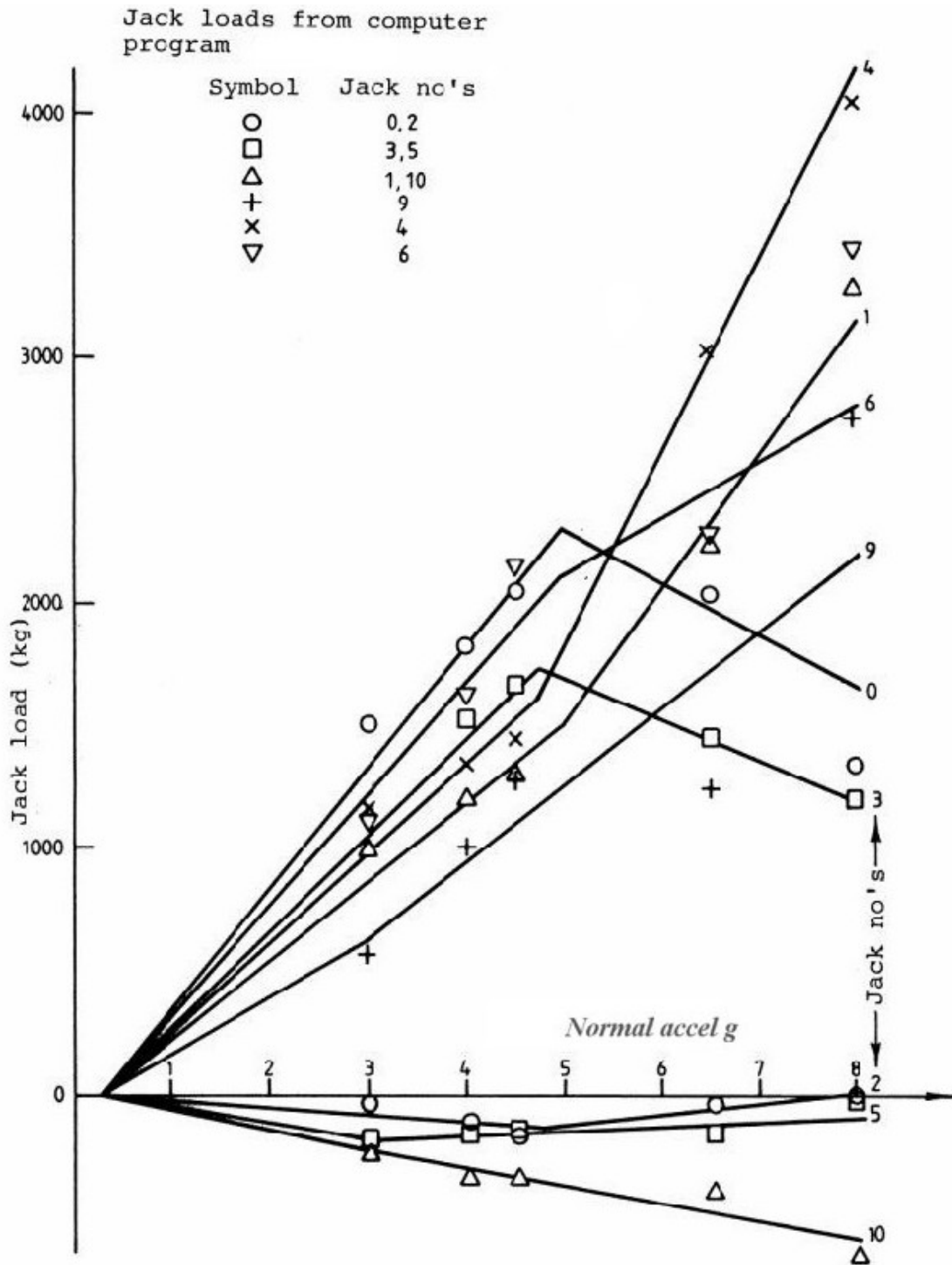
The mathematical structural model (mentioned in Section 4.1) was used early in the test preparation stage to derive nodal loads from one general load case, which allowed preliminary design work to proceed. The result indicated that twelve jacks would be required. Eleven jacks would apply loads to the wing (six above and five below), and one jack to simulate fuselage bending. This was achieved by applying a vertical deflection to the rear spar at its connection to the "dummy" fuselage.

As the structural modelling program was developed, and adjusted by ground calibration and flight test data, it was able to derive the nodal load distribution (from known flying conditions), and calculate the associated end loads in the structural members of the theoretical model.

For each nodal load distribution, the jack load could be determined by summing the nodal loads within its area of influence. Through the jack's "whiffle" tree system, the resulting loading pad loads could be calculated. Using these pad loads as inputs to the model, member end loads were calculated and compared with those of the associated nodal load distribution. Jack loads were adjusted to improve the agreement, so that stresses in the main spar and adjacent front spar were within 2% of the maximum member stresses calculated from the associated distribution.

This process of calculating jack loads was not done until the whole Mirage flying load spectrum of 3700 hours of data was consolidated into nine load cases (eight manoeuvre and one gust), (see Section 5). Of the eight manoeuvre cases, six were completed as outlined above. The remaining two cases (containing only a small number of loads above 3g that contributed relatively little calculated fatigue damage), were completed by a more approximate procedure.

Jack loads were plotted against normal acceleration for each load case. For load case 6, a pair of straight lines was fitted to each series of points (Figure 21). This relationship of jack load and normal acceleration was used as read only memory (ROM) for the computer sequence load tape (Section 6). The change in sign of the slope of some pairs of lines arises from changes in centre of pressure position at high angles of attack. The line fitting was performed manually to ensure best fit in the region 3g to 6g, which contained the most damaging loads. As indicated in Figure 21, the lines were constrained to pass through a small positive normal acceleration value at zero jack load. This was necessary because at zero normal acceleration some elevon load was required to balance the aircraft (Ref.27). The above procedure was not used to calculate jack loads for negative 'g' manoeuvre because test loads were applied by single acting jacks. It was considered acceptable to apply the relatively few negative loads by one downward acting jack that was situated near the end of the main spar. The jack load versus 'g' relationship was established from strain measurements in the test rig and from in-flight readings (Ref.29).



Note: Loads in jacks 7 and 8 were insignificant for this load case

Figure 21: Jack Loads versus g for Load Case 6 (See Ref.16 for details of jack loads program)

## 5. Load Sequence

This section is a condensation of Ref.30 in which a full data description is given along with the methods used to reduce it for use in the fatigue test.

The test specification called for a flight-by-flight load sequence that would within the constraints of time and funds available, accurately simulate all load conditions that caused significant fatigue damage to the wing as operated by the RAAF.

### 5.1 Service conditions

Initially the load cases considered were:-

- a. manoeuvre loads;
- b. air brake loads;
- c. gust loads;
- d. thermal effects;
- e. ground loads (ie. landing, take-off and taxiing); and
- f. and fuel tank pressurisation loads.

As discussed in Section 4.3.3, air brake loads were neglected. Earlier flight tests indicated that thermal stress effects were negligible. Therefore they were ignored.

### 5.2 Service data

Fatigue meters had been fitted to the fleet when the aircraft entered service. In addition to recording load exceedances, the data sheets gave information for each flight, type of flight (ie. mission description), fuel tank and weapons configuration at take-off. A considerable database (some 110,000 hours) of RAAF usage had been gathered. However the test was based on 1971-72 data (see Section 5.5) which provided a total of 37,000 hours. A further sixteen flights supplemented the data that covered the operational usage of the fleet. A continuous record was made of normal acceleration, Mach number, airspeed, altitude and fuel weight. It was considered that these sixteen flights, with some specific reservations, could be regarded as being representative of (the then) current flying practice and provided a basis for the sequence of normal acceleration and load turning points.

### 5.3 Data reduction

All the data had to be reduced onto a magnetic tape that would control the test. For practical purposes, the length of this tape was to be five hundred flights of approximately one hundred cycles per flight.

This data reduction was achieved by taking the sixteen continuously recorded flights as a base for sequencing the load cycles in each of the various missions of squadron

usage. The wide range of flying conditions enabled the recorded flight data from the various missions to be grouped in similar flight profiles (ie. altitude, Mach number and load histories).

Each group could then be identified with one or more of the sixteen flight load sequences on the basis of:-

- a. discussing the flight profiles and loading severities with RAAF aircrew;
- b. examining the sixteen flight data records; and
- c. comparing damage rates calculated from fatigue meter data for various combinations of flight, fuel and weapons.

This work resulted in nine mission groupings, covering fifty-five combinations of type of flight, fuel and stores configuration<sup>3</sup>. Most groups contain missions of the same purpose but differed in fuel and weapons used. Some missions differed in purpose but had similar flight profiles and loading histories. Other combinations that occurred less than once per thousand flights were not explicitly represented.

#### 5.4 Manoeuvre load cases

The flight load distribution over the wing varied considerably with changes of altitude, Mach number, fuel and stores configuration. Thus the relative stresses throughout the wing were continually changing. Fuel usage was predictable because tanks were emptied in the same sequence. Weapon delivery also followed a repeatable pattern. To allow for these changes in stress caused by flight parameters, the flight profiles for each mission group were split into two or more segments having characteristic Mach number and altitude, but short enough in duration for fuel usage effect to be small.

This segmentation of the nine mission groups of fifty five configurations, resulted in a total of 137 flight segments, each identified by Mach number, altitude, weight, fuel and stores configuration. These segments were consolidated into twenty-eight groups of equivalent segments on the basis of wing root bending moment at mid-flight (Ref.27).

To reach a further reduction in the manageable number of load cases (from twenty-eight segment groups), software developed by the CAC was used to obtain data at the wing root. This consisted of:-

- a. predicted flight load distributions;
- b. bending moment;
- c. shear;
- d. torque; and
- e. stresses in all areas of the wing likely to be fatigue critical, especially in the main, and front spars.

---

<sup>3</sup> As the control tape length was 500 flights, an event occurring more than once per 100 flights would be greater than 0.5 in 500 flights and hence be considered as an integer.

Segments with similar root bending moments and stresses (each calculated at 3g) were collected into eight groups such that in highly stressed areas of the spars, the tolerance on stress was generally +/-4% while tolerance on moment was +/-2.5%. From each group one characteristic segment was selected to represent that group. These eight segments defined the eight manoeuvre load cases to simulate all manoeuvre loads. These are shown in Table 2. A further load group was added to cover the gust load case.

Table 2: Consolidated manoeuvre load cases

Load case	Altitude × 1000 (ft)	Mach no.	Indicated air speed (kt)	Fuel code	Weapons code	Fuel weight (kg)
1	35	0.90	310	065	05	1196
2	35	0.90	310	071	00	1261
3	3	0.72	450	099	00	1580
4	14	0.85	440	071	00	1261
5	3	0.72	450	065	02	1196
6	14	0.85	440	065	01	1196

## 5.5 Representation of manoeuvre load sequences

In general, a representative load sequence from one of the sixteen recorded flights was chosen. The load magnitudes were modified to realistic levels for each turning point in the load sequence. This was done to be consistent with the appropriate fatigue meter data.

The relative frequency and mission allocation of each of the sixteen flight load sequences was determined by the usage breakdown for 1972.

The test load spectrum for each mission group (as defined by the number of exceedances of various normal acceleration thresholds), was to be consistent with the 1971-72 fatigue meter data. These requirements could not be met by the sixteen recorded flight load sequences which consisted of only 20 hours compared with 37,000 hours of fatigue meter data.

The load sequences were therefore modified using the following assumptions:-

- a. operational requirements of each group remained consistent, so that the general pattern of manoeuvres was repeatable;
- b. magnitude of load turning points could be amplified or attenuated due to the differing handling qualities of aircraft and pilots; and
- c. small adjustments were permitted for a few individual turning points.

## 5.6 Mission sequence

Examination of fatigue meter records showed that the order of flights was not entirely random. Further analysis enabled correlation between any two consecutive flights and the probability of similar flight run lengths to be established. It was decided to preserve (as far as possible in the block of five hundred flights), the order existing in service usage. To this end the sequence of missions was reduced to two groups of frequencies. The first showed the frequency with which the subject mission was followed by a different mission. The second showed the frequency of occurrence of the various run-lengths. Runs of ten identical missions were common and one case of 40 was observed which could be explained by an extension of training sorties and a desire to minimise changes to aircraft configuration. The analysed data related to 18,877 flights, which were compressed to 500 for the test.

The resultant test sequence conformed to the statistics built into its construction, but it could not contain the rarer events, which existed in the original data.

## 5.7 Truncation of load sequence

A fatigue test has to simulate service load conditions in a laboratory within the time scale imposed to reach the desired result. The time taken to complete a test comprises the running time and down times (either scheduled or un-scheduled).

The main factor governing running time is the number of applied load cycles to reach failure. Load cycles of small magnitude are numerous and where required to be reduced in frequency for this test. This was done but with caution as they were considered to be important in the crack initiation stage and in re-sharpening the crack tip after large magnitude loads have been applied.

The load spectrum was truncated at the lower end to eliminate the load cycles with amplitudes less than 0.38g. Below this value, the calculated fatigue damage was negligible.

A Mirage test life of 9,000 flights was required within four months of test start date. With an average load cycle frequency of 0.33Hz, and an assumed running efficiency of 25%, the maximum allowable cycles per flight were 100.

The practical physical length of the load sequence tape had a storage capacity of  $1.4 \times 10^6$  instructions. With twelve jacks, each requiring 200 instructions per flight, a maximum tape length of 500 flights was possible. The top load of 7.8g was recorded on the control tape only once in an interval of 500 flights. While this load was not the highest load applied to the wing, it did produce the largest bending moment at the wing root. The maximum positive load applied to the wing was 8.45g, which was expected to occur once in any mission category during the expected service life of the wing (ie. 5,000 flight hours). This load was applied by punched paper tape input to the

computer. It was planned to apply the load once every 5,000 flights or after 10 repeats of the control tape. The load was applied during the test six times in 32,373 simulated flights, but not at regular 5,000 flight intervals (see Figure 4).

The load spectrum was further truncated on the negative side by the inability of the rig to apply loads less than  $-1.0g$ . The rate at this level was 6 per 500 hours.

## 5.8 Ground load representation

Because the purpose of the fatigue test was to determine the life of the wing, it was necessary to apply only those undercarriage loads that would cause significant damage to the wing. Therefore only the vertical component of the landing, taxiing and take-off loads were applied. In addition, a drag or "spring-back" load was applied. This load was considered important because high speed photographic records taken during landing trials of a Mirage aircraft showed a severe backwards deflection of the leg on impact followed by a "spring-back" as the wheel came up to speed at the first bounce. The result of this load gave a shock into the wing structure. It was achieved by applying a 1,400kg drag load to the axle of the wheel in conjunction with a vertical applied load of 3,400kg, then the drag ("spring-back") load was suddenly applied by triggering a "bomb" release lock ("hook").

Figure 22 shows the sequence and magnitude of these loads and the lever system that provided a loading platform under the wheel that was supported on rollers to allow for relative movement as the wing and oleo leg deflected. The ground loads were derived from three sources, namely the manufacturer's acceleration spectrum for taxiing, RAAF flight tests in which an oleo leg was instrumented to give a magnitude outline and the sequence of undercarriage loads. In conjunction with these data was the assumption that the take-off weight was 10,500kg and the landing weight was 8,000kg. A detailed loads derivation rationale is found in Section 8 of Ref.30.

## 5.9 Wing fuel tank pressurisation

In the aircraft the pressurisation cycle of the wing fuel tank (Figure 23) was controlled by the operation of the engine. Under normal conditions this would coincide with the start and finish of a flight. Therefore in the test, the fuel tank chamber within the wing was pressurised to 58.6 kPa (8.5 p.s.i.) at the start of a simulated flight and depressurised at the end of the flight. This pressure was used as the midpoint in the operating range of the aircraft's pressure reducing valve.

Filtered air from a normal industrial compressor (pressure capacity of 552 kPa [80 p.s.i.]) was used with a number of safe guards to prevent over charging of the wing. The main precaution against over-pressure was to fill the wing from a storage tank with a capacity (upon discharge into the wing) equalised to the required pressure. A series of interlocking and pressure regulating valves provided added protection in the event of malfunction.

A water manometer was used as a safe and simple overload device and as an accurate visual check on the air pressure being applied to the wing. An additional pair of pressure switches were used, one to signal the start of the pressure cycle to the computer and the other as an electrical over-pressure device to operate the emergency dump valve No. 4 (Figure 23).

A schematic diagram of the system is shown in Figure 23. This figure lists the sequencing of the solenoid valves during the four stages of the pressure cycle. The starting and sequencing of these valves was under the management of the load control tape.

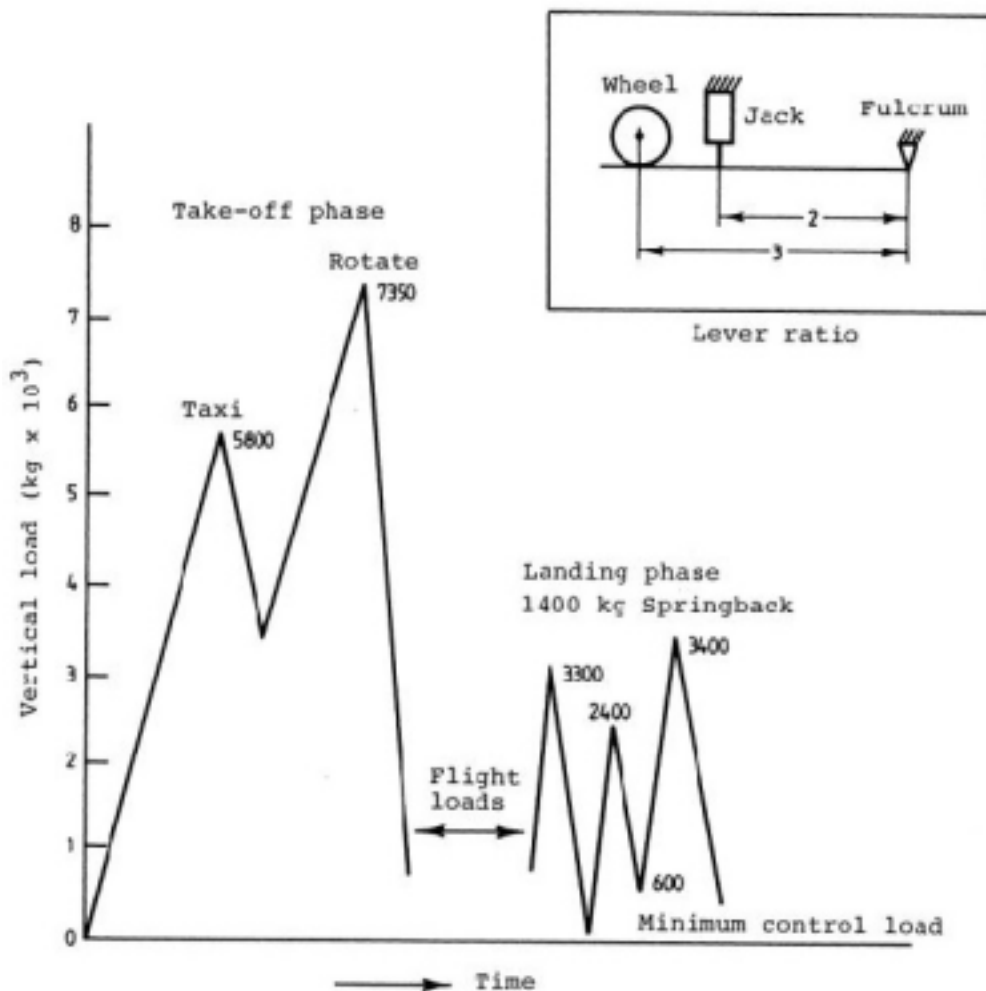


Figure 22: Undercarriage Load Sequence. Note a load sequence was applied during application of landing load sequence (see Figure 20)

### 5.10 Flight-by-flight load representation

Of the one hundred load cycles (on average) per flight, four were ground loads that included gust loads. The remaining load cycles were proportioned to 40% manoeuvre and 60% gust.

At the start of each flight, while the taxiing and take-off loads were applied [Figure 22], the fuel tank was pressurised and the wing loaded as shown in Figure 20. The load cycling commenced with gust and manoeuvre loads applied in a random sequence according to the particular flight being represented. On completion of those loads, the wing was again loaded as shown in Figure 20, while the landing loads were applied and followed by the “spring-back” load. The fuel tank was then de-pressurised, ready for the start of the next flight load sequence. Note that the “spring-back” load was applied at the end of the landing load sequence instead of the beginning of the sequence because it caused a shock to the loading system that could have introduced transient faults, resulting in the stoppage of the test rig.

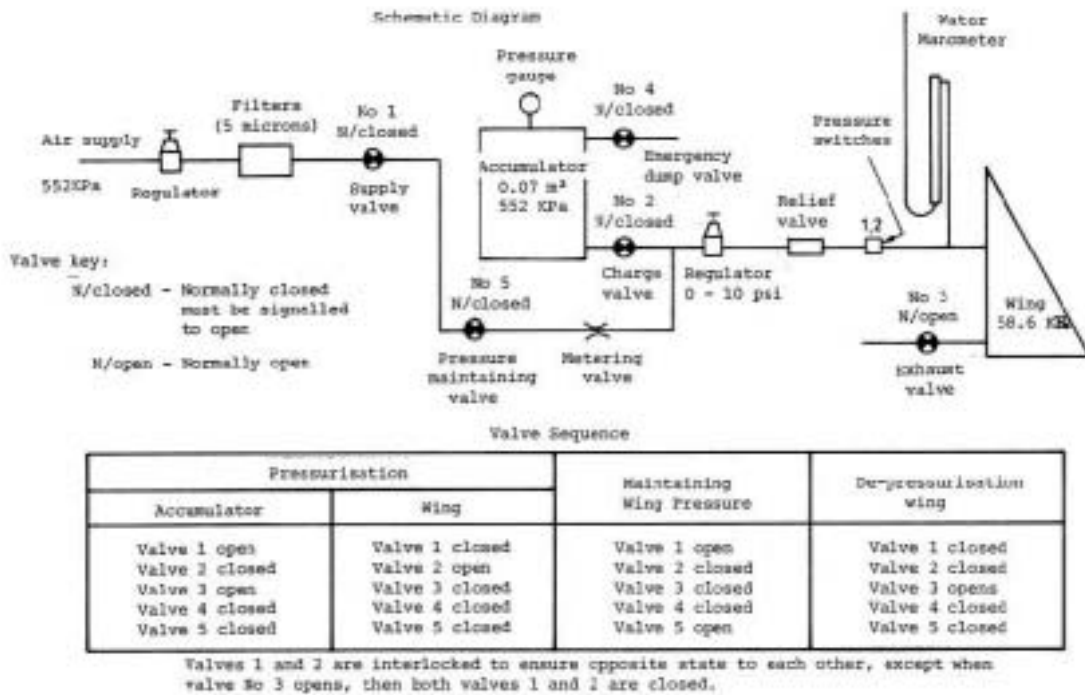


Figure 23: Pressurisation Schematic of Wing Fuel Tank

### 5.11 Load sequence applied during test

It was intended to apply the loading sequence (flights 0 to 500 on the control tape) without interruption, even if a control fault occurred during a flight. Upon restarting of

the load sequence, the computer was programmed to continue from the previously applied load. Table 3 shows the actual load history applied during the test.

Table 3: Flight load history of Mirage wing fatigue

Date of last flight	First flight in programme	Last flight in programme	Date of last flight	First flight in programme	Last flight in programme
18-Jan-74	1	2	2-Aug-74	1	154
21-Jan-74	1	22	3-Aug-74	206	500
25-Jan-74	1	161	6-Aug-74	1	500
5-Feb-74	1	1	9-Aug-74	1	500
6-Feb-74	1	4	12-Aug-74	1	500
7-Feb-74	1	32	14-Aug-74	1	500
7-Feb-74	1	1	15-Aug-74	1	281
	100	126	16-Aug-74	1	1
	33	115	18-Aug-74	286	500
10-Feb-74	127	500	20-Aug-74	1	500
17-Feb-74	1	500	21-Aug-74	1	258
5-Mar-74	1	500		186	188
7-Mar-74	1	370	23-Aug-74	259	500
7-Mar-74	1	1	26-Aug-74	1	500
8-Mar-74	402	500	28-Aug-74	1	500
	1	17	31-Aug-74	1	500
11-Mar-74	16	500	3-Sep-74	1	225
15-Mar-74	1	500	5-Sep-74	274	500
18-Mar-74	1	500	7-Sep-74	1	500
21-Mar-74	1	500	10-Sep-74	1	500
24-Mar-74	1	500	12-Sep-74	1	500
26-Mar-74	1	500	14-Sep-74	1	500
28-Mar-74	1	500	16-Sep-74	1	500
30-Mar-74	1	452	19-Sep-74	1	258
31-Mar-74	1	208		1	1
2-Apr-74	1	500	20-Sep-74	245	500
4-Apr-74	1	500	22-Sep-74	1	500
7-Apr-74	1	500	8-Oct-74	1	500
8-Apr-74	1	500	27-Sep-74	1	500
26-Apr-74	1	500	29-Sep-74	1	500
29-Apr-74	1	500	1-Oct-74	1	500
	1	19	3-Oct-74	1	500
1-May-74	1	500	5-Oct-74	1	500
3-May-74	1	500	7-Oct-74	1	426
7-May-74	1	500	8-Oct-74	1	212
9-Mar-74	1	500		1	1
11-May-74	1	500	9-Oct-74	212	500
15-May-74	1	500	11-Oct-74	1	500
17-May-74	1	500	14-Oct-74	1	394
19-May-74	1	500	15-Oct-74	1	5
21-May-74	1	500	16-Oct-74	1	176
23-May-74	1	463	18-Oct-74	183	500
27-Jul-74	1	500	20-Oct-74	1	500
29-Jul-74	1	500	21-Oct-74	1	500
1-Aug-74	1	500		1	64
1-Aug-74	1	45	21-Oct-74	**	

\*\* Failure of spar halfway through 65.

## 6. Control Tape

A PDP11 computer was used to store the test load sequences from the 500 flights and the data were used to derive the load magnitude for the various load channels. The results of this then provided the load distribution for each load turning point.

### 6.1 Creation of control tape

A load sequence control tape enabled the computer to calculate the test loads from its stored data. A separate tape was also created to commission the rig.

The method and parameters used to generate the resultant wing load distributions has been described in Section 4.3.5 and shown diagrammatically in Figure 17. Section 4.3.6 described how this load distribution was applied to the wing using 12 jacks and associated whiffle trees. This section outlined how a relationship was derived between jack load and normal acceleration. Thus knowing the type-of-flying, the fuel, weapon stores, a load distribution could be applied to the wing for every 'g' acceleration (ie. every load turning point).

Section 5 outlined how service flying was reduced to eight manoeuvre and one gust load case, and the operational mix of these cases. The load turning point within each manoeuvre case was also obtained from a continuous record of sixteen flights covering the operational range of the fleet. These data were coded and stored in the computer so that they could be recovered by the control tape which contained the following input data for each load turning point:

1. Code number specifying the aircraft fuel configuration (Table 4);
2. Code number specifying the aircraft stores configuration (Table 5);
3. Code number specifying the type-of-flying (Table 6);
4. Centre of gravity normal acceleration;
5. Mach number;
6. Altitude;
7. Pitch acceleration;
8. Aircraft's instantaneous fuel weight;
9. Undercarriage loads;
10. Turning point reference number; and
11. Expected readings of four strain gauges on the wing (reference purposes only).

Table 4: Fuel configuration codes

Code	Fuel configuration
048	Internal tank
053	Internal tank + gun bay tank (GBT)
056	Internal tank + 1 by supersonic tank (110 gal)
062	Internal tank + GBT + 1 by 110
065*	Internal tank + 2 by 110
070	Internal tank + 1 by 286 gal
071*	Internal tank + GBT + 2 by 110
074	Internal tank + 3 by 110
076	Internal tank + GBT + 1 by 110
077	Internal tank + 1 by 374 gal
080	Internal tank + GBT + 3 by 110
083	Internal tank + GBT + 374
088	Internal tank + 1 by 286 + 2 by 110
093*	Internal tank + 2 by 286
094*	Internal tank + GBT + 1 by 286 + 1 by 110
095	Internal tank + 2 by 110 + 1 by 374
099*	Internal tank + GBT + 2 by 286
101	Internal tank + GBT + 2 by 110 + 2 by 374
102	Internal tank + 1 by 110 + 2 by 286
107	Internal tank + 2 by 374
108	Internal tank + GBT + 1 by 110 + 2 by 286
113	Internal tank + GBT + 2 by 374

\* Denotes most frequently used configurations.

Table 5: Weapons configuration codes

Code	Weapons configuration
00	No weapons
01	Gun or practice bombs
02	Guns + practice bombs
03	Sidewinders (or rails)
04	Matra (or pylon)
05	(Guns or practice bombs) + Sidewinders
06	Guns + practice bombs + Sidewinders
07	Sidewinders + Matra
08	Sidewinders + Matra + guns
10	500 lb HE bombs
11	Guns + 500 lb HE bombs

Table 6: Type of flight (TOF) codes

Code	Title	Remarks
00	Local flying	Circuits, etc. Seldom used.
05	General flying	Instrument flights, conversion flights.
10	Transit (medium or high level)	Ferry, high navex, high-low navex, strike.
20	Transit (low level)	Low navex, tac. recce., photo recce.
30	Test flying	Engine test, post-service tests.
40	Formation flying	Seldom used.
50	Tactical maritime exercises	Seldom used.
60	Unidentified	Undefined flights. Seldom used.
70	Aerobatics	Display flights, and training for these.
80	General intercept	High or low intercept
81	Tactical intercept	Air combat tactics
82	Air-to-air gunnery and cine	-
90	Ground attack	Weapons delivery.
	SPECIAL CODES FOR THE TEST	
	* 06 Negative load case	
	* 07 Landing load case	
	* 08 Gust load case	
	* 09 Pressure load case	

## 6.2 Verification of control tape

A further V-g-h data tape was produced after verifying that the frequency of loads was not counted by the fatigue meters between  $-0.5g$  and  $+2.5g$ , and the simulation of linking manoeuvres. This investigation showed close agreement between the control tape (used in the test) and the operational usage of the aircraft. A detailed account of this work is reported in Appendix 1, Ref.30.

## 7. Design and manufacture of test rig

The test rig (Figure 24) design and manufacture was divided between CAC and the GAF. CAC was tasked to handle all aspects of the dummy fuselage and derivation of theoretical wing load distributions. GAF was involved with the design, manufacture, and erection of the wing and undercarriage loading systems. Outlines a description of the rig, together with the sources of data and the basis of the design.

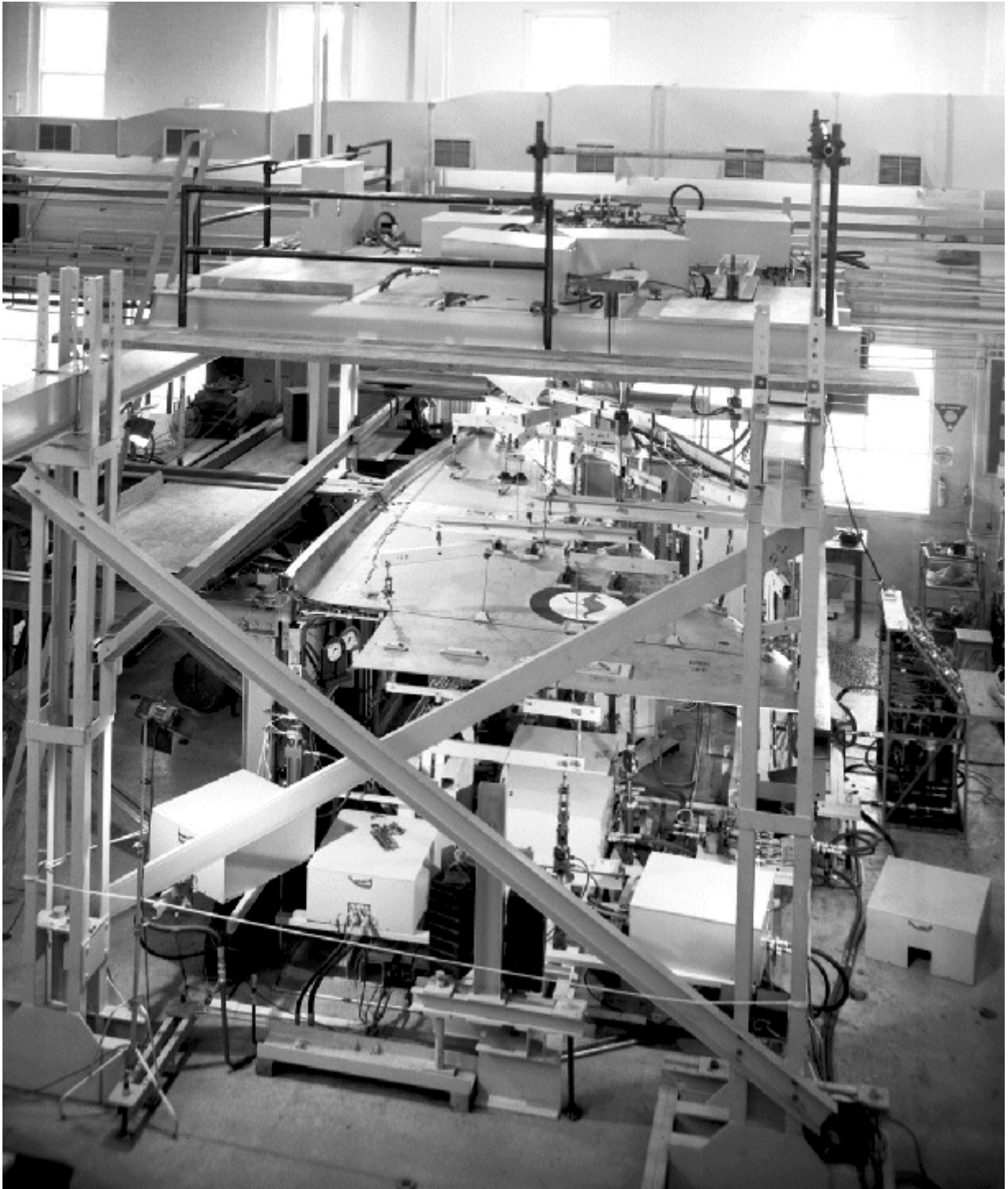


*Figure 24: General View of Test Rig*

## 7.1 Hydraulic actuator control system

ARL staff in the Instrumentation and Structures Experiment Group of Structures Division undertook the design and development of the valve packs which controlled the flow of high pressure oil into and out of each actuator. Appendix C provides some details of the valve pack system. The load system for the Mirage wing fatigue test had the ability to change the load distribution over the wing at every load turning point. The combination of a computer and a multi-channel servo system was used to produce a complex, continually varying load pattern.

# 8. Test Article Inspections

A detailed account of the inspection procedures carried out during the test is given in Refs 15 and 31. In brief, there were four types and they were all based on routine service practise and periodicity. They were:-

1. Daily inspection

A visual inspection of all accessible areas while the load cycling was in progress, using fluorescent penetrants and low power magnifying glasses as required.

2. 'A' inspections (every 250 flights)

With the test load held at 1g, a visual inspection (as 1 above) was made and areas around critical fastener holes were inspected using eddy-current techniques and dye-penetrants. Ultrasonic techniques were used along lower spar flanges.

3. 'B' Inspections (every 750 flights)

The wing was removed from rig (see Appendix B). Inspections as outlined in 2 (above) were repeated and followed by an inspection of the main attachment pinholes, using a magnetic rubber replication technique. On refit of the wing, a refurbished pin and split-sleeve assembly was fitted.

4. 'C' inspection (every 2250 flights).

The wing was again removed and inspection 3 (above) was repeated. In addition, X-ray radiographs were taken of selected areas along the main spar and leading edge spar that were inaccessible by other methods.

Figure 4 shows in tabular and graphical form when these inspections were actually done.

The 'C' inspection was the most important and difficult to perform. Initially it took three men over three shifts (72 man-hours) to complete, but with experience, this was

reduced to 27 man-hours. After the 25<sup>th</sup> 'B' inspection, the X-ray inspections were discontinued, as they were time consuming and found to be of doubtful value.

Loss of air-pressure from the pressurised tanks was also found to be a valuable indicator of crack development.

## 9. Data Acquisition

The test wing was strain gauged at 80 measuring stations, Figure 8. The wing was then flown to obtain in-flight data for use in the derivation of applied loads, and to provide the basis for rig calibrations before being fatigue tested.

### 9.1 Static Strain Surveys

At intervals during the test, sets of load increments were applied to the wing and strain records taken for all stations. A strain per 'g' gradient for critical locations was determined from these loadings and these locations were monitored during the test. This was done in order to detect any changes in load distribution through the wing structure. In particular, it was hoped that interpretation of these data would indicate the initiation of final failure, however subsequent events showed that this was not possible for the failure that caused collapse.

These runs were made using all of the 80 strain gauge stations as a check on the integrity of the structure and to detect changes in load path distributions through the wing. A total of 52 calibration runs were taken during the test, six at the start of the test, and then 19 up to 15,455 flights (when the first major skin panel crack was found. Five more cracks were found during the subsequent 60-day down-time, and 22 more cracks during the remaining 16,917 flights).

Of the 19 runs taken between the start of the test and the discovery of the first major crack, only three are comparable, and they were irregularly spaced, the last occurring at 4,178 flights. The other 16 runs were taken during an investigation into loading along the rear spar.

Four of the five runs at 15,455 flights were inconclusive because there were wide variations in strain between gauges that could not be reconciled. These data showed steady trends up or down in response to progressive changes in load, and re-distribution through the wing structure as damage occurred.

### 9.2 Continuous recorded strain data

There were fourteen channels available on the test control computer for continuous recording of data at each load turning point as a means of monitoring the applied test

loads. Of these, one was used for wing tip deflection, seven for monitoring actuator loads and six for strain gauge data. Initially the six strain data stations were: two aileron actuators (106 and 107), front and aft flange faces of the main spar root (16.1 and 16.2) and the aft lower flange at two spanwise positions (1.4T and 2T).

At 15,455 flights a crack in the fuel tank panel was discovered (Ref.15). It was decided to gather more strain data during the final stages of the test. This was achieved by deleting the two aileron actuators and three load actuators. The fourteen positions continuously recorded were then:

2T, 1.4T, 16.1, 16.2, 222T, 217.3, 38S (2 channels), 1 deflection, 4 load actuators, 0, 1, 3, and 5 (Table 7, Appendix B) and 223T (a new gauge station installed on the lower spar boom directly opposite where the crack in the panel was expected to end).

A new gauge replaced one of the load actuators, 16.5, that was added to the main spar root at 20,627 flights. Unfortunately analysis of these data subsequently showed that it was not reliable, particularly for gauges 223T, and 222T (see Ref.33).

## 10. Test Article Failures

A full description of failures that occurred during the test is given in Ref.15. They are briefly described here.

Figure 26 shows all the fatigue cracks that were found in the wing with the exception of the cracks in the upper surface, forward of the main spar. Final failure occurred at hole Z. Final failure locations in the French spar test and the port wing failure in the Swiss full-scale test are also shown.

Cracks were found in four bolt holes in the rear lower spar flange at D, E, A and B and one crack 'C' in the forward lower flange of the main spar. Likewise, cracks were also in the lower rear flange (G and F) from two holes for rivets that attached the anchor nut plates.

Fatigue cracking in the skin occurred in 4 places. The major cracking was from a fixed anchor nut hole. When found at 15,455 simulated flights, it was 27mm long. Its final length was 469mm (Figure 26).

In a pre-test inspection, cracks were found in the upper skin forward of the main spar. These cracks occurred in service aircraft and were refurbished by a standard repair scheme that was incorporated with a modification in the same area. Therefore at 9,514 flights, the repair scheme was applied to the upper skin of the test wing.

Nine cracks were found from seven holes in a skin panel attached to the forward lower flange of the main spar just outboard of final collapse. These cracks were considered to be minor in extent and were discovered at 17,000 flights (52% of total life).

A crack 23 mm (in length) was found from the fuel decant hole. This crack passed through a countersunk rivet hole towards the root rib at approximately 45 degrees to the main spar. Discovery of this crack occurred subsequent to the test due to reports of cracks being found in the same area in service aircraft. A boron fibre patch repair scheme was developed (and tested on the Swiss F&W fatigue test) for this area (Refs 35, 36 and Figure 25) and successfully applied to extend the service life of fleet aircraft.

During the examination of all these cracks, efforts were made to determine crack initiation from a study of the fracture surface. This was a difficult and time-consuming study that could be done only on the fractured surface at final failure.

## **10.1 Final failure**

Final failure and collapse of the wing occurred after 32,372 flights (31,230 simulated test flights plus 1,142 pre-test equivalent flights) at the blind hole in the lower boom of the main spar (Figure 27 and Figure 28) 433 mm from the centre of the main spar attachment holes. It occurred unexpectedly under a load of 7.8g, during flight 65, load case 7, which simulated air combat tactics mission. This load, whilst not the highest in g value, did produce the greatest bending moment in the spar because of the aircraft loading conditions. The calculated nominal stress at this load was 151 MPa (21,800 p.s.i.). This cracking was not subsequently detected in-service aircraft (probably due to the earlier cracking in the anchor nut rivet holes).

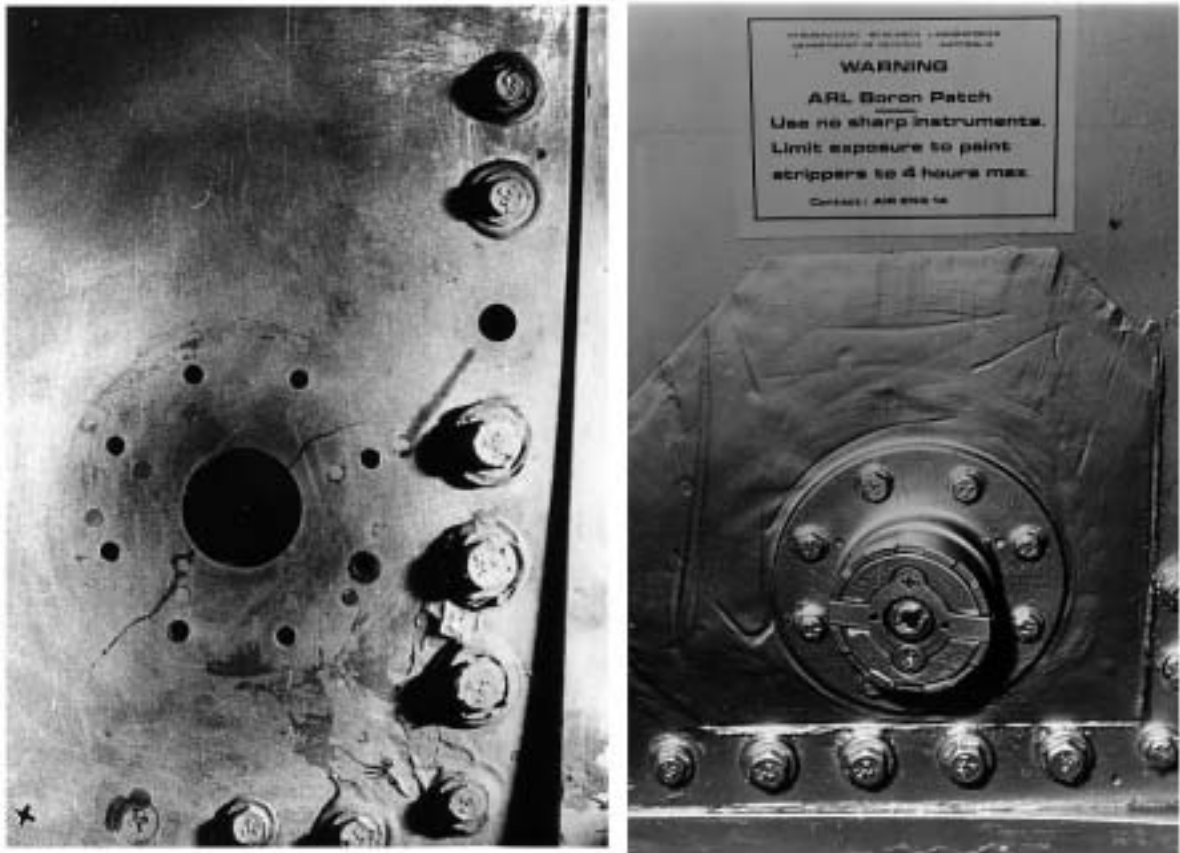


*Figure 25: In-service Cracked Mirage Lower Wing Panel before and after Boron/epoxy Patching (see Figure 26 for equivalent test failure details)*

The crack originated from a dimple at the bottom of a hemispherical hole that had not been removed during manufacture. This hole contained a threaded insert into which one of the fixed fairing attachment screws fitted. This crack was not detected before collapse even though inspections were made along the spar at regular intervals during the test.

Because the load sequence was random, the factographic examination of the crack propagation rings on the fracture surface was not straightforward (Figure 28). Subsequently a new method based on fracture mechanics (Ref.37), was developed. This model of the crack propagation process was assumed to predict crack front positions from the final crack (front) back to smaller crack sizes. From this computer model program, a theoretical estimate was made of the crack growth that would predict initiation to be early in the life of the wing (Figure 29). Unfortunately the theoretical curve did not agree with that measured in the early stages of crack growth. Because of the limitations in the theoretical model, it was more reasonable (in the early stages of crack growth) to favour the initiation point suggested by the method of crack front measurement. This gave an estimate of 20,000 flights for crack initiation to a detectable

size, resulting in a crack propagation period of 12,372/32,372, giving 38.2% of total life to failure.

The relevant scatter factors to be applied to the results of Mirage wing failure were carefully studied and outlined in an explanatory note by eminent ARL scientists in Appendix D.

Subsequent to the fatigue test several related analyses were conducted (Refs 33 to 58).

## **10.2 Cracks in lower rear flange bolt holes**

Crack D, Hole 1 (Figure 26) was suspected at the same time as crack E, Hole 2 at 15,455 flights. This was not confirmed until the holes were broken open for closer examination. This showed that the cracks in each hole did originate from fretting and had propagated during the test. The fracture faces of these holes showed the regular repetition of marks found in the face of the crack that caused final collapse.

Crack A, hole 12, crack B, Hole 11 and crack C forward flange, were found when the spar was stripped after final collapse. Cracks D and E propagated from the lower forward edge of the bolt hole ie. web side. Crack B propagated from the lower and upper aft edges of the hole. Cracks A and C propagated from the lower aft and forward edges. The aft side of crack A being the largest of all cracks.

## **11. Conclusion**

A broad historical description has been given of the different phases (planning, flight testing, rig construction, testing and data collection) of the Australian Mirage III0 wing fatigue test conducted at Fisherman's Bend. This provides a record of what was an innovative and successful fatigue test program. Much of the technology developed in this program forms the back-bone of subsequent programs even today. This program also led to in-service crack patching which significantly extended the service life of aircraft.

## **12. Acknowledgements**

The editors gratefully acknowledge the useful discussions with, and contributions from, A. Machin, T. van Blaricum, Vui Tung Mau and R. Pell of Air Vehicles Division.

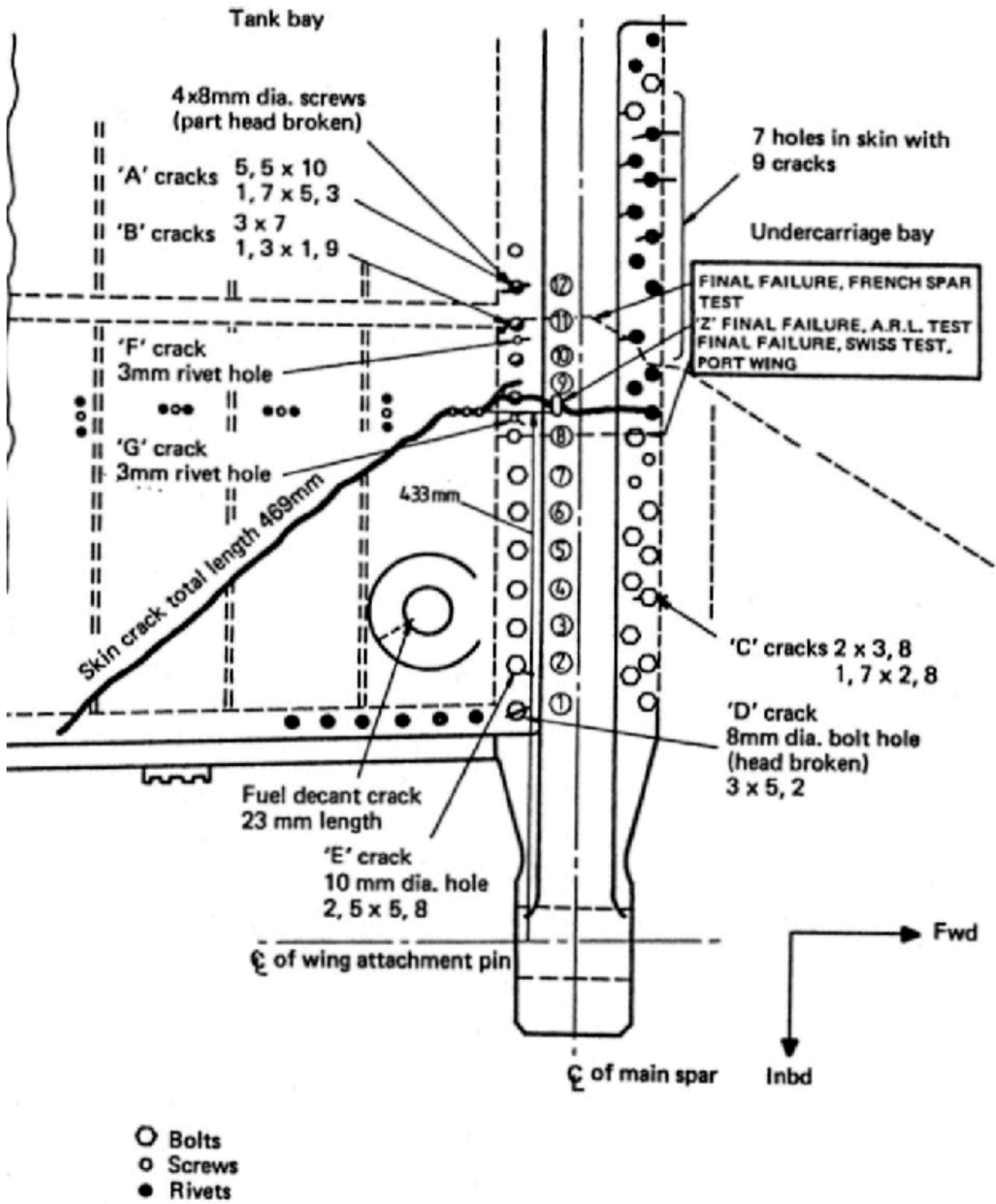


Figure 26: Failure Locations in Starboard Mirage Wing Viewed from Lower Surface



*Figure 27: General View of the Final Failure in the Main Spar Lower Flange*

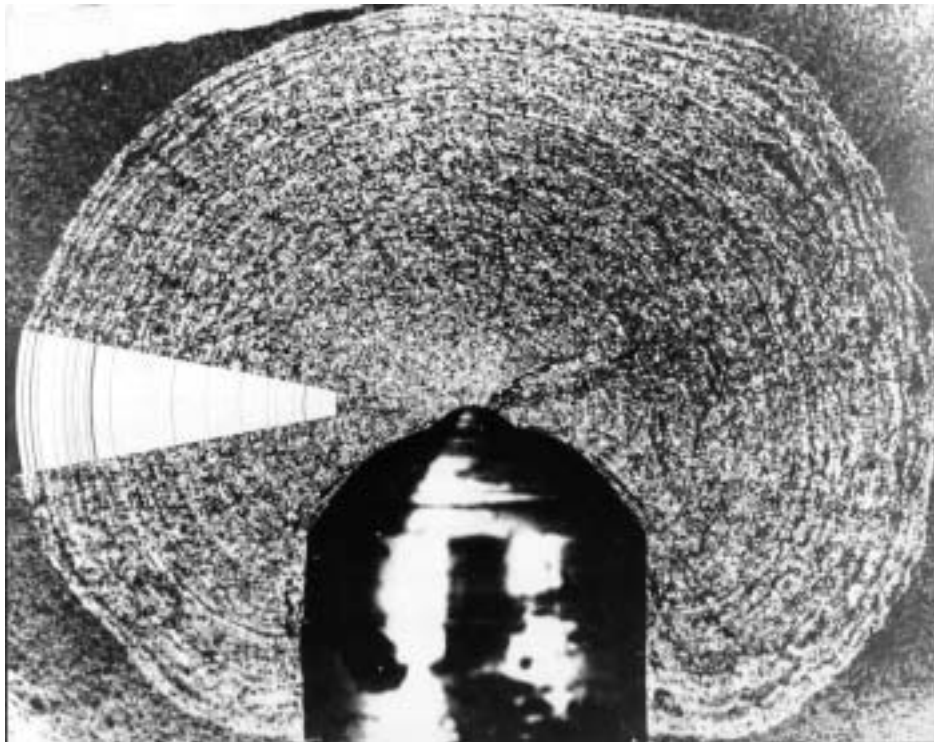


Figure 28: Close-up View of Failure Location showing Fatigue Crack Progression Markings and those Predicted by Quantitative Fractography

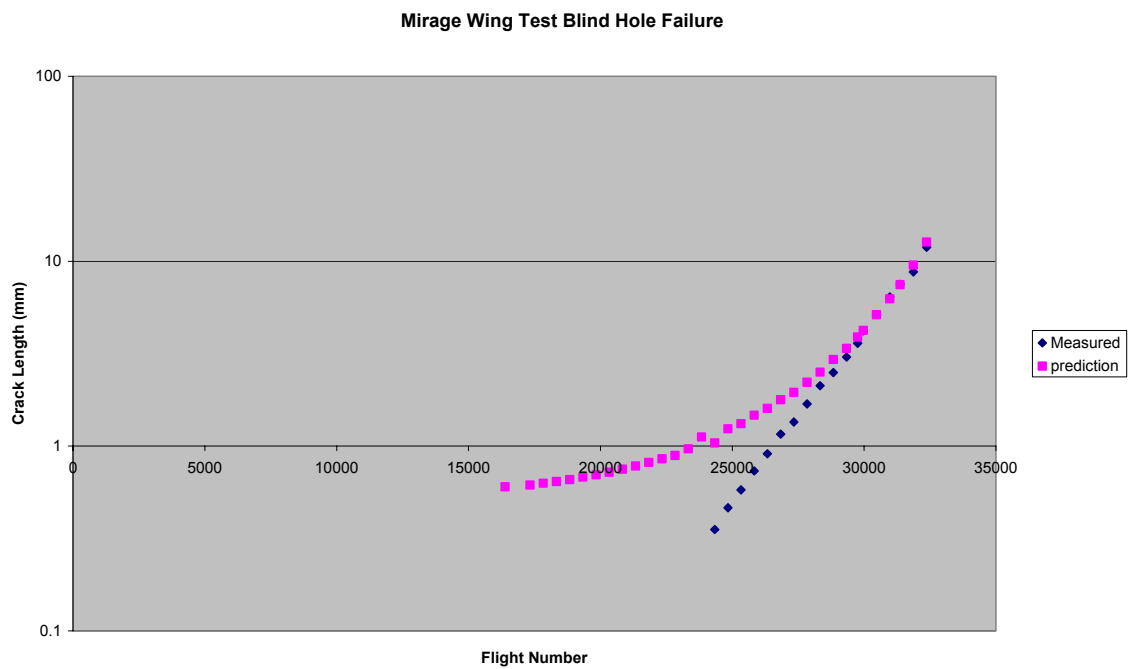


Figure 29: Fractographic Measurements versus Predicted Crack Growth (from Ref.37)

## 13. References

1. Essai en fatigue de longeron principal - Mirage IIIC. Generale Aeronautique Marcel Dassault. Report No. NC3027 April 1963.
2. Gee, S.W., Mirage Stage 1 fatigue investigation Part II. Gauging Mirage III aircraft for flight testing. Aero Res Labs Structures Note 343, Jan 1969.
3. Higgs, M.G.J., Mirage Stage 1 fatigue investigation Part IV. Curve Fitting of Transducer Calibrations. Aero Res Labs Structures Note 339, Jun 1969.
4. Townshend, P.H. and Watts, N.C., Mirage Stage 1 fatigue investigation Part V. - Calibration of undercarriage. Aero Res Labs Structures Note 337, Jun 1969.
5. Moody, E.S. and Denehy, D.R., Mirage Stage 1 fatigue investigation Part III. Instrumentation of aircraft. Aero Res Labs Structures Note 348, Jan 1970.
6. Paterson, A.K., Sherman, D.J. and Thomson, M.R., Mirage Stage 2 fatigue investigation Part I - The Data Recording System. Aero Res Labs Structures Note 380, Sept 1972.
7. Coyle, J.J., Load calibration of Mirage III0 elevon and rudder control system, Structures Tech Memo 242, Mar 1976.
8. Patching C.A. and Townshend, P.H., Mirage Stage 1 fatigue investigation - Static ground calibration of aircraft. Structures Note 468, Aug 1980.
9. Howard, P.J., Patching, C.A. and Payne, A.O. Life estimation by parametric analysis. Proc. Eighth ICAF Symposium, Lausanne, May 1975, pp. 4.3/1 - 4.3/28.
10. Mirage III - essai statique generale, montee a charge limite. Marcel Dassault. Note de Calcul No. 250.
11. Repartition de pression sur demi-module 1:25 Vol. 4. Resultant de pressions extrados - intrododos. Eidgenossisches Flugzeugwerk Emmen, Bericht FO 919/4 April 1969.
12. Landers, E.R.A and Edwards, D.A., Wind tunnel tests on a 1/50<sup>th</sup> scale model of the Mirage III-0 aircraft, Part 1 Tests at Supersonic Speeds. Weapons Research Est. Tech. Note 415 (WR&D), June 1971.

13. Landers, E.R.A and Fenton, C.E., Wind tunnel tests on a 1/50<sup>th</sup> scale model of the Mirage III-0 aircraft, Part II Tests at Mach No's from 0.40 to 0.95. Weapons Research Est. Tech. Note 735 (WR&D), August 1972.
14. Rider, C.K., Thomson, M.R. and Verinder, F.E. Measurement of extreme mechanical turbulence during low level flights by Mirage A3-76. Aero Research Labs Structures Report 333, May 1971.
15. Bruton, R.A., Failures resulting from a fatigue test on a Mirage IIIO wing. Aero Research Labs Structures Tech Memo 319, July 1980.
16. Beckett, R.C., Mirage wing fatigue test - the results of pre-test wing inspection. Commonwealth Aircraft Corporation Report AA306 1973.
17. Beckett, R.C. and Leung, K.C., Mirage wing fatigue test - test predicted strains and deflections in pre-flight load calibration. Commonwealth Aircraft Corporation Report AA279 Nov. 1974.
18. Beckett, R.C. and Szarski, L., Mirage wing fatigue test - derivation of pickup loads from measured strains. Commonwealth Aircraft Corporation Report AA273 Mar. 1978.
19. Keays, R., Mirage wing fatigue test - strain survey - proposed calibration loading. Commonwealth Aircraft Corporation Report AA.376, 1978.
20. Beckett, R.C. and Szarski, L., Mirage wing fatigue test - Derivation of wing loads from measured strains. Commonwealth Aircraft Corporation Report AA274 Mar. 1978.
21. Skopinski, T.H., Aiken, W.S. and Huston, W.B., Calibration of strain gauge installations in aircraft structures for measurement of flight loads. NACA Report 1178,1954.
22. Hovell, P.B., Webber, D.A. and Roberts, T.A., The interpretation of strain measurements for flight load determination. Aeronautical Research Council Current Paper No. ARC839, Aug. 1964.
23. Leung, K.C., Mirage wing fatigue test - mathematical structural model. Commonwealth Aircraft Corporation Report AA278 Nov. 1973.
24. Nankivell, J. and Beckett, R.C., Mirage wing fatigue test - theoretical wing loads distribution. Commonwealth Aircraft Corporation Report AA276 Jan. 1973.
25. Beckett, R.C., Mirage wing fatigue test - wing fuselage fairings and their effects. Part I. Commonwealth Aircraft Corporation Report AA271 Oct. 1972.

26. Beckett, R.C., Mirage wing fatigue test – wing fuselage fairings. Part II. Commonwealth Aircraft Corporation Report AA272 Oct. 1972.
27. Beckett, R.C., Mirage wing fatigue test – analysis of test load conditions. Part I. Commonwealth Aircraft Corporation Report AA277 Mar. 1973.
28. Beckett, R.C., Mirage wing fatigue test – analysis of test load conditions. Part II. Commonwealth Aircraft Corporation Report AA301 Sep. 1974.
29. Minutes of Mirage Fatigue Test Committee Meeting 21<sup>st</sup> December 1973. Aero Research Labs file B2/03/3.
30. Grandage, J.M. and Howard P.J., Mirage IIIO wing fatigue test – Development of load sequences. Aero Research Labs Structures Note 460, June 1980.
31. Bruton, R.A., Mirage wing fatigue test – main spar attachment fittings, problems and remedies. Aero Research Labs Structures Tech Memo 267, Aug. 1977.
32. Ludowyk, C.J. and Moody, E.S., Application of electro-hydraulic control to fatigue testing. Aero Research Labs Structures Note 412, Nov 1974.
33. Howard, P.J., Sparrow, J.G. and Thomson, M.R., Strain distribution in the Mirage main spar. Aero Research Labs Structures Note 464, Oct 1980.
34. Beckett, R.C. and Szarski, L., Mirage wing fatigue test. Test article pre flight load calibrations. Commonwealth Aircraft Corporation Report AA270 Nov. 1972.
35. Baker, A.A., Callinan, R.J., Davis, M.J., Jones, R. and Williams J.G., Application of BFRP crack patching to Mirage III aircraft, J. Theoretical and Applied Fracture Mechanics 2, 1-5 (1984).
36. Van Blaricum, T.J., The repair of cracked aluminium alloy panels using boron fibre reinforced patches. Aero Research Labs Structures TM 404, July 1985.
37. Anderson, B.E. and Goldsmith, N.T., Prediction of crack propagation in Mirage wing fatigue test spar. Aero Research Labs Structures Note 448, Apr. 1978.
38. Goldsmith, N.T., Fractographic examinations relevant to the F&W Mirage fatigue test, Aero Research Labs -Mat-Tech-Memo 371.
39. Howard, P.J., Fatigue damage due to gust loading of Mirage III0. Aero Research Labs Structures Note 428, June 1976.

40. Grandage, J.M., A reassessment of the ARL and Swiss Mirage fatigue test lives. Aero Research Labs Structures Note 468, Dec 1980.
41. Hoskin, B.C., Callinan, R.J., Jones, R., Interim damage tolerance analysis of Mirage frame 26; stress distribution, critical areas and critical crack sizes. Aero Research Labs Structures Technical Memorandum 356, Jan 1983.
42. Mann, J.Y., Kaelin, R. and Wilson, F.E., Extending the fatigue life of a fighter aircraft wing, Aircraft Fatigue in the Eighties, Netherlands National Aerospace Laboratories, 1981.
43. Mann, J.Y., Lupson, W.F., Machin, A.S., and Pell, R.A., Interim report on investigation to improve the fatigue life of the Mirage III0 wing spar, ARL-STRU-TECH-MEMO-334, 1981.
44. Mann, J.Y. and Jost, G.S., Stress fields associated with interference fitted and cold-expanded holes, Metals Forum 6, 1983.
45. Mann, J.Y., Machin, A.S, Lupson, W.F. and Pell, R.A., The use of interference-fit bolts or bushes and hole cold expansion for increasing the fatigue life of thick-section aluminium alloy bolted joints, ARL Structures Note 490, Aug 1983.
46. Mann, J.Y., Machin, A.S., Lupson, W.F. and Pell, R.A., Techniques for increasing the fatigue life of thick-section aluminium alloy bolted joints, Aluminium, Volume 60, number 7, pp 515-520, Jul. 1984.
47. Mann, J.Y., Pell, R.A., and Machin, A.S., Fatigue crack propagation in Mirage III0 wing main spar specimens and the effects of spectrum truncation on Life, ARL-STRUC-R-405, 1984.
48. Mann, J.Y., Machin, A.S., Lupson, W.F., Improving the fatigue life of the Mirage III0 wing main spar. Aero Research Labs Structures Report 398, Jan. 1984.
49. Finney, J.M., Harris, F.G., Pell, R.A., Dentry, C.S. and Stefoulis, C.T., Modelling for fatigue crack growth prediction in Mirage 1110, frame 26, ARL-STRUC-REP 401, Apr. 1984.
50. Machin, A.S., The residual strength of cracked specimens representing a section of the Mirage III0 wing main spar, ARL-STRUC-REP-408, 1984.
51. Mann, J.Y., and Revill, G.W., A Comparison of fatigue lives under a complex and a much simplified flight-by-flight testing sequence, ARL-STRUC-TM-388, 1984.

52. Mann, J.Y. and Revill, G.W., Fatigue lives of specimens representing critical locations in Mirage III spars under Australian and Swiss test spectra, ARL-STRUC-R-415, 1985.
53. Mann J.Y. and Kennedy, K.J., A case study in fatigue life extension - the main spar of RAAF Mirage 1110 wings, Mech. Engng Trans., I. E. Aust, 1985.
54. Mann, J.Y., Pell R.A. and Machin, A.S., Some aspects of variability in fatigue crack initiation and propagation in thick aluminium alloy sections, International Journal of Fatigue, Volume 7, Number 2, 59-66, Apr. 1986.
55. Pell, R.A., Beaver, P.W., Mann, J.Y. and Sparrow, J.G., Fatigue of thick-section cold-expanded holes with and without cracks, Fatigue and Fracture of Engineering Materials and Structures, Volume 12, No. 6, p.p. 553-567, 1989.
56. Mann, J.Y., Machin, A.S. and Lupson, W.F., Further investigation to improve the fatigue life of the Mirage wing main spar, ARL-STRUC-TM 397.
57. Mann, J.Y. and Revill, G.W., A comparison of fatigue lives under a complex and a much simplified flight-by-flight testing sequence, ARL-STRUC-TM 388.
58. Clark, G. and Pell, R.A., Experimental and theoretical analysis of fatigue crack growth at fastener holes in an aluminium alloy, Transactions of Multi-Disciplinary Engineering, Special issue on Aerospace Engineering, Dec. 1992.
59. Beckett, R.C., Mirage wing fatigue test - effect of fuselage flexing on wing strains. Commonwealth Aircraft Corporation Report AA280, Nov. 1974.
60. Reed, M.L., Mirage wing fatigue test - description of wing reaction frame. Commonwealth Aircraft Corporation Report AA275, June 1974.
61. Payne, A.O., Determination of the fatigue resistance of aircraft wings by full-scale testing. Proc. (edit. F. J. Plantema and J. Schijve) Full-scale fatigue testing of aircraft structures, 5-11 June, 1959, Amsterdam, Peragon Press.

*This page is deliberately blank*



	63	Rear Spar Stn	Shear	10265-R2	10268-R4	CAC29-00603	10562-R3
	64	Rear Spar 500mm From Attach. Pin	Shear	10265-R2	10268-R4	CAC29-00603	10562-R3
	106	Actuator I/B Elevon Load	Stbd Actuator I/B	-	10268-R4	CAC29-00603	10562-R3
	107	Actuator O/B Elevon Load	Actuator O/B	-	10268-R4	CAC29-00603	10562-R3
Fairing Gauges Ref. Drg. 10267-R1	205	Near Front Spar Pick-up	Tension	10267-R1	10268-R4		10563-R1
	206	Near Front Spar Pick-up	Shear	10267-R1	10268-R4		10563-R1
	207	Near Main Spar Pick-up	Tension	10267-R1	10268-R4		10563-R1
	208	Near Main Spar Pick-up	Shear	10267-R1	10268-R4		10563-R1
	209	Near Main Spar Pick-up	Tension	10267-R1	10268-R4		10563-R1
	210	Near Rear Spar Pick-up	Tension	10267-R1	10268-R4		10563-R1
	211	Near Rear Spar Pick-up	Shear	10267-R1	10268-R4		10563-R1
	212	Near Front Spar Pick-up	Tension	10267-R1	10268-R4		10563-R1
	213	Near Front Spar Pick-up	Shear	10267-R1	10268-R4		10563-R1
	214	Near Main Spar Pick-up	Tension	10267-R1	10268-R4		10563-R1
	215	Near Rear Spar Pick-up	Tension	10267-R1	10268-R4		10563-R1
	216	Near Rear Spar Pick-up	Shear	10267-R1	10268-R4		10563-R1
	217	Bot. Skin Near Main Spar	Rosette	10723	10268-R4		10563-R1
	218	Bot. Skin Near Main Spar	Rosette	10723	10268-R4		10563-R1
	219	Top Skin Near Rear Spar	Rosette	10723	10268-R4		10563-R1
	220	Bot. Skin Near Rear Spar	Rosette	10723	10268-R4		10563-R1
	221	Front Spar Near Junction With Main Spar	Tens., Comp.	10723	10268-R4		10563-R1
	222	Main Spar Stn 450	Tens.	10263-R4	10268-R4		10562-R3
	223	Main Spar Stn 154	Tens.	10263-R4	10268-R4		10562-R3

## **Appendix B: Design and Manufacture of the Test Rig**

The test rig was divided into two structural sections, one that applied the loads and the other that reacted to the loads.

Part one consisted of portal frames above the wing from which were attached hydraulic jacks and their associated whiffle trees that applied the positive loads to the wing and undercarriage loading structure. Part two consisted of the “dummy” fuselage that reacted with all the applied loads.

The GAF designed, manufactured and erected part one of the test rig and CAC designed, manufactured and erected part two.

The placement of the jacks, whiffle trees, hydraulic load console and hydraulic reticulation system was completed by contract labour supplied by CAC. The company subsequently assisted in the commissioning and operation of the rig. shows a general view of the wing in the test rig.

### **Assembly of test rig**

The reaction frame was the first part of the test rig to be erected. This enabled an early check to be made of the wing fitment. Opportunity was also taken to test the validity of simulating the flexibility of the aircraft’s fuselage by vertically displacing the rear spar attachment point. This was followed by the erection of the columns and overhead loading beams. Concurrently, the tension pads and bolt-through load attachment fittings were fitted to the wing. The wing was then positioned in the reaction frame and a platform built over it for protection while overhead hydraulic jacks, associated piping and valve gear was installed. Similar hydraulic loading equipment was installed under the wing.

In a separate and specially designed rig, each servo controlled loading channel (jack load cell, servo-valve, servo amplifier and control valves) was tested and tuned before being fitted into the loading frame. This rig consisted of a number of leaf springs and masses that could be varied to simulate the reaction forces within the wing area that was loaded by each jack. The unloading rates were set on the rig. They were essential to prevent overloading of any one area of the wing in the event of a fault occurring in the multi-channel loading system. Two such rigs were built to shorten the time to check each of the fourteen load channels.

As each load channel was fully checked and set, it was installed in the test frame, ready for connection to the wing through its own whiffle tree system. The completion of this assembly work was exacting and time consuming. Every part had to be operating correctly to give confidence in load control before commissioning could start. As

outlined in Figure 4, this work was planned to take 4.5 months but had to be extended by an additional 2.5 months.

**Loading frame**

As mentioned in Section 4.3, an early theoretical load distribution based on six flight load cases was made to initiate rig design. Three sources of data were used for this work, namely GAMD design office calculations, Swiss wind tunnel investigations and the results from early ARL test flights.

It was decided from this theoretical study that 51 loading points could cover the range of load distribution, 22 were tension pads and 29 were bolt-on fittings. Table 7 lists the coordinates of each jack, its associated set of loading points and the type of fittings used. Figure 30 outlines the wing loading attachment fittings.

An easily definable datum on the wing was used to assist in accurate positioning of the loading points. To simulate the forward component of the lift force caused by the angle of attack to the wing, the anchorage point of the positive loading jacks was moved forward to give the loading system a 5-degree inclination to the vertical. The maximum negative load was applied by a single jack at the end of the main spar, through the attachment fitting for the supersonic fuel tank. The magnitude of this load was limited to 454 kg by the strength of this hard point. A constant drag load of 360 kg created by this tank was applied by dead weight acting in a rearward direction using a pulley and cable loading system.

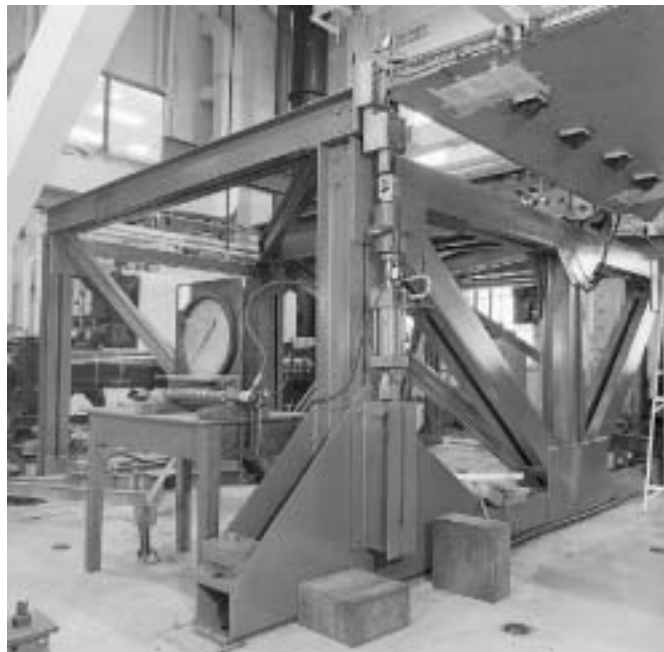
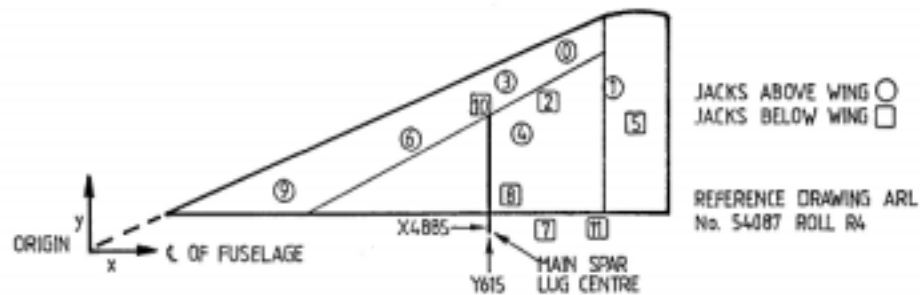


Figure 30: Wing Test Rig Dummy Fuselage Showing Two of Four Attachment Locations

Table 7: Jack and loading point co-ordinates



Jack No.	Associated loading points				Jack No.	Associated loading points				
	No.	Type	co-ordinates			No.	Type	co-ordinates		
			X	Y				X	Y	
①	1	Bolt	6791	3632	①	6	Bolt	7045	3848	
	2	Bolt	6813	3519		7	Bolt	7460	3836	
	-	-	6408	3395		8	Bolt	7045	3669	
	3	Bolt	6302	3338		-	-	7105	2747	
	4	Bolt	5982	3172		9	Bolt	7449	3609	
5	Bolt	5860	3033	10		Bolt	7045	3104		
②	14		6186	2853		11	Bolt	7045	2504	
	-		5958	2764		12	Bolt	7045	1903	
	15		5776	2692		13	Bolt	7045	1259	
④	21	Pad	6187	2654		③	16	Bolt	5693	2959
	22	Pad	5773	2656			17	Bolt	5532	2859
	23	Pad	5323	2507	18		Bolt	5237	2661	
	24	Pad	6188	2310				5017	2554	
	25	Pad	5774	2312	19		Bolt	4740	2468	
-	-	5644	2266	20	Bolt		4258	2079		
④	26	Pad	5349	2312	⑤		31	Bolt	7537	2685
	27	Pad	4860	2144			-	-	7547	2531
	28	Pad	4966	1881			32	Bolt	7557	2312
	29	Pad	5788	1882			33	Bolt	7571	1898
	30	Pad	5370	1881		34	Bolt	7593	1482	
⑥	35	Pad	4509	1944	⑦	44	Pad	6635	1112	
	36	Pad	4395	1868		-	-	6415	1111	
	37	bolt	4377	1501		45	Pad	6186	1110	
	38	Bolt	3732	1836	⑧	46	Pad	5072	1329	
	39	Bolt	3601	1742		47	Pad	5774	1152	
	-		3910	1645		-	-	5350	1234	
	40	Pad	3954	1455		48	Pad	5359	1154	
	41	Pad	3875	1572		49	Bolt	2601	1290	
	42	bolt	4130	1046		50	Bolt	2648	1198	
43	Pad	3790	982	-	-	2481	1113			
⑩		Bolt	4885	2250	⑨	60	Bolt	2199	961	
						⑪		Slide	7030	658

### **Tension pads**

Loads were applied through tension pads (Figure 31) located at critical areas of the wing. This method was selected because:

- (a) the wing skin was relatively thick;
- (b) it gave a reasonable distribution of point loads into the skin;
- (c) it did not create any stress concentrations; and
- (d) it provided a weak link in the applied load path in the event of an overload.

Considerable care was taken to ensure that no hydraulic oil from the overhead jacks fell on the wing surface because of possible effects on the adhesive strength and life of the tension pads. The use of tension pads proved quite successful however there were six failures in four pads. The two highest stressed pads (rubber loaded to 45% of ultimate strength) failed twice. Failure repairs were easy to undertake at the rate of two hours per pad.

In the less critical areas along the leading edge where the loads were high and curvature of the wing surface considerable, the load link was terminated in a length of chain that was connected to a 'through-bolt' fitting. Along the rear spar a rod replaced the chain.

The undercarriage loads were applied through a complete oleo leg and wheel to simulate the correct load distribution into the main and front spar trunnion bearings.

A jack applied the vertical load through a lever system (Figure 22). The wheel rotated on a platform that was free to move on rollers in a spanwise direction, thus preventing a side load being applied as the oleo leg and wing deflected. A jack attached to the wheel axle (via an electrically operated bomb release) applied the "spring-back" load.



*Figure 31: Wing Upper Surface Loading Pads*

### **Reaction frame**

The wing was attached to a dummy fuselage at four points, ie leading edge, front, main and rear spars, (see Figure 24, Figure 32 and Figure 33). A study of the deflections is reported in Ref.10, while confirmatory calculations are reported in Ref.59. The leading edge and front spar vertical deflections were shown to be due to fuselage bending, but these were small and could be ignored. The rear spar vertical deflections however were found to be significant. Hence it was decided to design for an extremely rigid reaction frame and simulate the flexibility at the rear spar by mounting its attachment lug on a sliding block that would be moved by a deflection commanded servo-hydraulic jack. Correct fuselage flexibility was simulated if and when a positive (ie upwards) load was applied to the wing, the lug being deflected downwards by an amount of 1 mm per g, (Ref.59).

The main spar wing-to-fuselage joint was designed to react bending, torsion and shear loads. Therefore it was the most critical design that was designed for a fatigue test life of 196,000 hours and consisted of two high tensile steel side plates that represented the split frame No. 26 of the fuselage, (Figure 32). The upper and lower attachment holes in these steel plates were bushed with an aluminium alloy similar to that used in frame No 26. The leading edge attachment points are shown in Figure 33.



*Figure 32: Main Spar and Undercarriage Side Link Attachment Points on Dummy Fuselage*

Another feature of this reaction frame was the wing root fairing support structure which was a necessary complication because flight strain results (Section 4.3.2) had shown that the fairings were capable of transferring a significant load directly from the wing to the fuselage, thus bypassing the lower joint.

The steel structure of the reaction frame was designed to be built in large prefabricated sections that could be transported from CAC to ARL and then bolted together. During erection, a wing master gauge was used to ensure correct alignment of the four attachment points. A full description of the reaction frame design is reported in Ref.60.



*Figure 33: Leading Edge Attachment to Dummy Fuselage*

### **Wing removal structure**

At regular intervals during the test the wing had to be removed from the “dummy” fuselage to facilitate inspection of the main spar attachment lugs. This was achieved by fitting under the wing, two double rail tracks that were fixed to the reaction frame at the inboard ends and to the portal frame at the outboard ends, (Figure 34). These tracks were orientated parallel to the main spar and positioned to give one support point on one track forward and two support points on the rear track, aft of the main spar. These three points were spaced apart to give a stable support platform to the wing and able to withstand the concentrated loading.

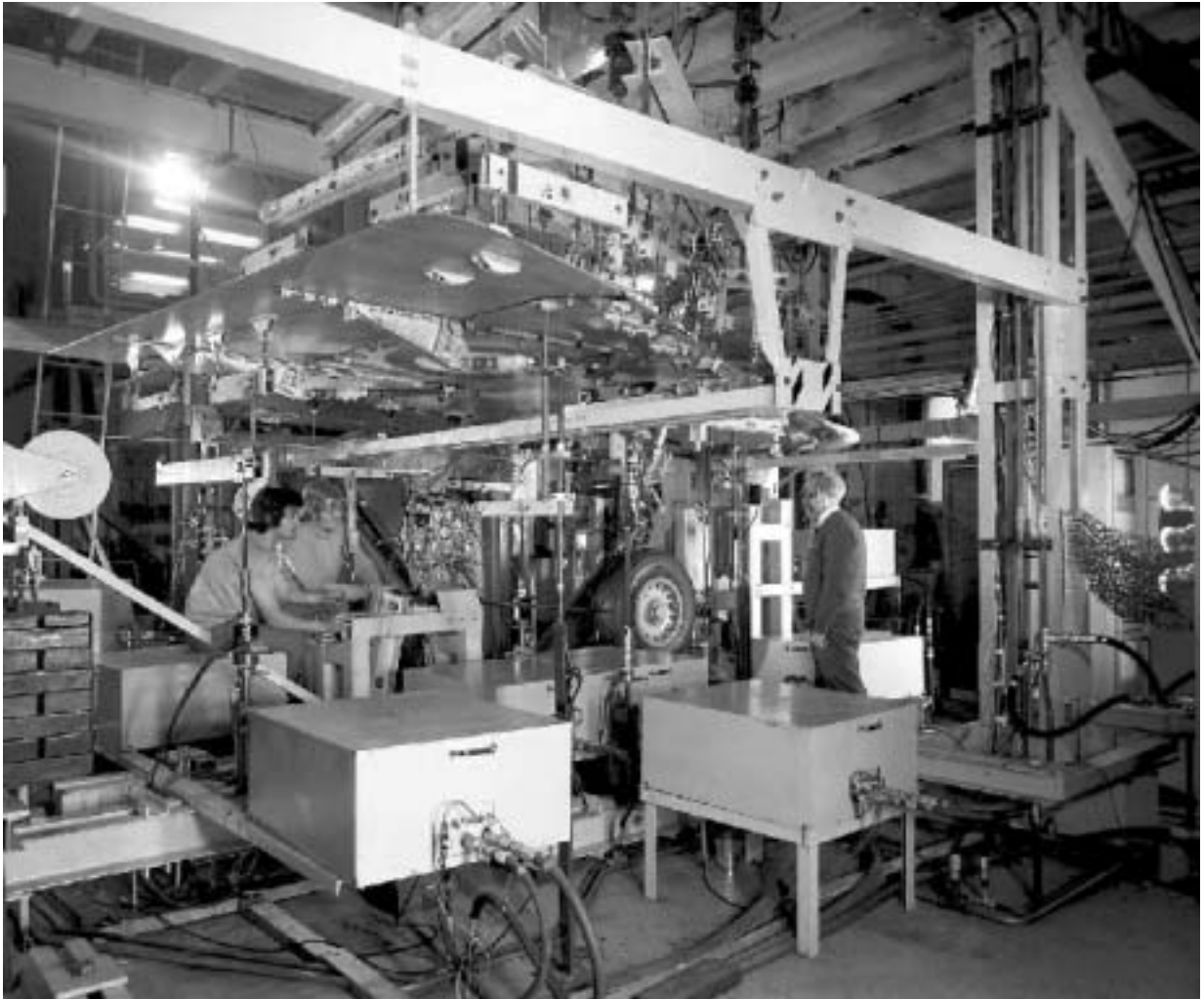


*Figure 34: Wing Lower Surface showing Wing Removal Rails and Drag Load System*

At each point, a toolmaker's screw jack was used to give vertical height adjustment. The span-wise and chord-wise directions of each jack were achieved by fixing the jack to a moveable platform on a 3-wheeled trolley. Both the platform and trolley movements were controlled by screw threads; the former in the chord-wise and the latter in the span-wise direction.

When the wing was to be removed, its weight would be taken on the 3 screw jacks. Great care was taken not to apply any twist to the wing that would reduce still further the very small side clearances between the main spar and side plates of the attachment point in the reaction frame. The spar attachment pins were then removed and the wing rolled out. The span-wise movement of the wing necessitated the disconnection of the under wing loading points only since they had been made stiffer in their "pinned" joints than their counterparts above the wing. This was done to prevent instability in

the servo controlled load system at the change-over-point from upward to downward loading.

### **Test running**

The test began with normal daytime running until all systems were tuned to give accurate and reliable operation. Three-shift operation was then implemented and continued until completion of the test. Three periods (see Figure 4) were an exception, cycling was stopped while decisions were made and repairs undertaken.

Four teams of three men, all CAC staff, operated the test rig on a 24-hour day, seven-day week schedule. In addition, key ARL staff were “on-call” over the nine months of actual testing to rectify faults in the hydraulic and computer control areas.

### **Test problems and remedies**

At the first ‘B’ inspection, difficulty was experienced in extracting the main spar attachment pins. These comprised a slotted parallel sleeve expanded by an internal tapered pin. On re-fitting of the pins, maximum allowable torque was required on the nuts (45m da N) to achieve the required interference.

Difficulties were again met at the removal for the second ‘B’ inspection. Excessive fretting had occurred in the bore of the lower main spar attachment hole. The area affected was considerable, with the deepest pit measuring 0.015 mm. The upper hole was also damaged but to a far lesser extent. The cause of this fretting, while initially thought to be the result of wrongly fitted pins, was finally attributed to two other factors.

1. The “Molycote” protective agent was spread as a film coating but was too thick and uneven which prevented the pins from maintaining sufficient interference.
2. Difficulty was experienced in reaching correct penetration before the maximum pull-in torque was reached.

Measurements were taken of the bore of the bushings in the dummy fuselage that represented Frame 26 of the aircraft. It showed that the diameter of the bushing holes were less than the spar holes. While this mismatch was very slight, it was highlighted by the fact that the aluminium alloy aircraft, (Frame 26), had been simulated in the test rig by two steel plates, Figure 30, fitted with aluminium alloy bushes which would require a larger force to achieve the same interference. The fretting in the spar holes was removed by aluminium oxide 400 grit abrasive paper and the wing reassembled into the rig.

At the third ‘B’ inspection, it was decided to enlarge the holes in the dummy fuselage by 0.0051 mm. No further trouble was experienced in achieving either correct fitment

or removal of the pins for the remainder of the test. The edge radius of the slit along the split sleeve was increased to 1 mm during this inspection period.

Two further changes were made:

- The thread in the tapered pin was re-tapped to a much coarser thread (1 1/8 inch BSF) to prevent stripping of this thread when using the pin extractor. A mechanical type pin extractor was made to suit this new thread size, replacing the hydraulic extractor.
- The angular position of the split sleeve was varied on the wing assembly to minimise the possibility of marking the bore of the wing spar holes.

At the completion of the test the condition of the boreholes in the spar was deemed as “good” (Figure 35), and still within tolerance for size and out-of-round. The surfaces of the pin-sleeve assemblies were also in excellent condition, which demonstrated the effectiveness of the “Molycote” film as a protecting medium.

A full account of these problems and recommended modifications is given in Ref.31.

Considerable trouble was experienced with the “bomb” release mechanism used to apply the undercarriage “spring back” loads. The fatigue performance of the mechanisms did not match the requirements of the test. Shortage of replacement parts and difficulty in repairs resulted in a reduced number of load cycles being applied during the last 3,000 flights.



*Figure 35: Lower Hole, Forward Face after Completion of Test*

### **Test system reliability**

The loading system took less time than predicted to become fully tuned and operationally reliable. Initial problems of control were encountered on two channels (No. 2 and 7, Table 7), because the actual test loads were smaller than forecast and more sensitive load cells had to be constructed and fitted. There were only minor problems with the computer.

The average rig cycling frequency was approximately 50 cycles per minute. The average testing rate was 13 flights per hour, with one test "flight" being equivalent to one hour of service flying, thus giving a time compression of 13 to 1.

Prior to 15,455 flights (Figure 4), when the rig was stopped for 61 days, the running efficiency reached 44%. This efficiency was based on an average possible cycling rate of 20 cycles per minute, 100 cycles per flight, giving theoretically 288 flights in any 24-hour period with no time allowed for scheduled inspections. When the test started again this running efficiency had dropped to 29%. At the completion of the test, the efficiency had recovered to 41%. Excluding time spent on regular inspections and mechanical maintenance, the efficiency of the system alone was greater than 70%.

*This page is deliberately blank*

## Appendix C: Actuator Control System (Valve Pack)

The function of this system was to control the hydraulic fluid entering and leaving each of the 12 load actuators. There were three control conditions to be satisfied:

1. Supply of oil pressure for load cycling;
2. Lock-up of actuators in the event of a system malfunction or structural failure (wing or loading system); and
3. Controlled simultaneous unloading of all actuators from any point in the load cycle following a system malfunction lock-up.

During normal load cycling, high-pressure hydraulic fluid from the main supply entered the valve pack through a “quick release” coupling. A woven mesh type stainless steel in-line filter strained the fluid as it passed to the electro-hydraulic servo valve (Figure 36). The servo valve distributed the fluid alternately to the tension and compression ends of the actuator (via the energised direction control valves (Sol V<sub>1</sub> and Sol V<sub>2</sub>) and through the energised pilot check valves (P/C V<sub>1</sub> and V<sub>2</sub>)). The servo valve was controlled by a varying command signal from the computer.

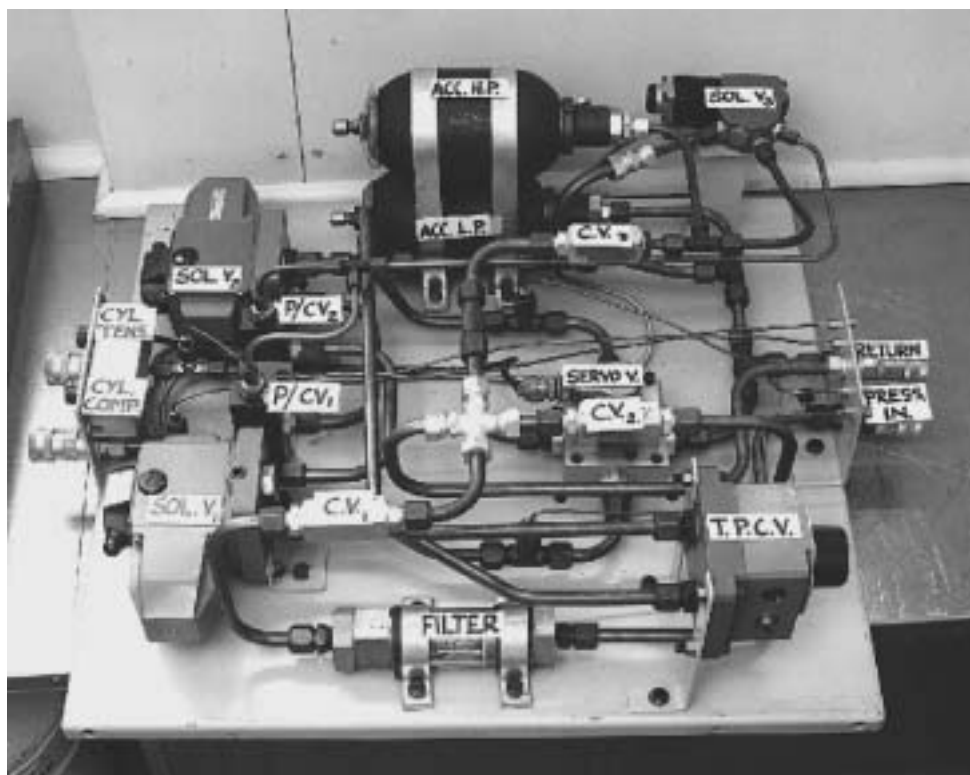


Figure 36: Actuator Control System (Valve Pack)

In the event of a control or hydraulic system malfunction, the specimen was held “locked” under the load at which this occurred. This was necessary to give time for the test personnel to clear the fault or safely unload the specimen. Without this protection, damage could be done to the specimen, particularly if one actuator should seize in the loaded condition, causing severe local stress to be applied to the specimen when the rest of the actuators remain unloaded. This lock-up capability also served as a fracture surface protection facility at the time of specimen failure. The fracture surfaces were held apart at failure, enabling the insertion of a soft plastic material before unloading; this protected the two faces from contact damage during unloading and subsequent dismantling.

If a fault occurred, the servo valve was instantly open circuited. This resulted in the main valve spool moving to the null position and blocking all fluid to the actuator. At the same time all solenoid valves were de-energised. Solenoid valves Sol V<sub>1</sub> and Sol V<sub>2</sub> blocked both the tension and compression lines from the servo valve to the actuator. Simultaneously, Sol V<sub>3</sub> de-energised the pilot operated check valves allowing a positive lock up of the actuator.

Unloading of the actuators, either individually or as a group, was accomplished by energising valves P/C V<sub>1</sub> and P/C V<sub>2</sub>. This was achieved (when required), by connecting the pre-charged accumulator Acc H.P. to the unloading circuit by energising Sol V<sub>3</sub>. The facility for individual actuator unloading was developed to permit “trimming” of the load distribution if found to be incorrect at lock-up, ie all actuator loads could be adjusted in correct proportion to the one with greatest negative error. To ensure controlled unloading of the actuators after lock-up, the loaded end of each actuator was connected hydraulically during unloading to a “Temperature and Pressure Compensated Control Valve” (TPCV).

As the volume at the tension end of the actuator decreased during unloading, so the volume at the compression end increased. Hydraulic fluid required to fill this increased volume at the compression end was drawn from the system return line via the de-energised Sol V<sub>1</sub>.

Such actuator control systems or “valve packs” were not commercially available at the time and were designed and manufactured by staff in the Structures Experimental Group. Later this form of control became the commercial standard.

### **Defining strategy of control system**

With the knowledge gained from overseas experience and locally conducted cantilever specimen tests, a control strategy was defined for the flight-by-flight load requirement.

In general, the principal factors required to achieve a higher cycling rate with small interaction loads were:

- a. high loop gain to detect small loop errors;
- b. wide loop bandwidth to permit rapid nulling errors; and
- c. a good margin of stability to prevent spurious oscillations.

Factor (c) above is usually mutually exclusive with factor's (a) and (b). From laboratory experiments performed, this was found to be especially so on the lightly damped cantilever test specimen. The experimental cantilever tests showed that the basic system was stable only at unacceptably low loop gains with a subsequent bandwidth of DC - 0.1Hz. Special compensation techniques were developed that permitted a threefold increase in loop gain, an increase in bandwidth to 4Hz while still maintaining a good stability margin. The success of this compensation scheme provided a measure of confidence that few problems would arise on the actual structure.

The cantilever tests provided useful evaluation data of other factors that influenced the system, eg:

- oil compressibility effects,
- backlash in linkages,
- effects of various parameters on servo valve null balance (eg. effect of oil leakage past jack piston seals).

All these effects were incorporated to involve a mathematical model of the system whose predicted results agreed closely with experimental results.

A control strategy was defined using the knowledge gained from the cantilever specimen test and from overseas techniques. This strategy was summarised as incorporating:

- a. load feedback control using double bridge load cells, with one used for load feedback loop and one to measure the load value for computer monitoring;
- b. lag compensation;
- c. "Null Pacing" of jacks (see below); and
- d. reset integrator switching at load excursion "dwell" plateaus.

Item (d) was a later development not incorporated in the early control strategy.

### **Design of control system**

With the system defined, specified sections of it were designed and built (eg. computer interfaces, servo-amplifiers, safety and control electronics, hydraulic control console and an actuator control system (valve pack).

The servo amplifiers were designed specifically for multi-channel testing with devices to improve load control accuracy at each turning point. A full operational description of the servo amplifiers is given in Ref.32. The computer software was programmed to

wait at each turning point for all channels to reach their commanded load value and signify a null, so called "null pacing".

The rate of change of command signal reduces as a turning point is approached in a closed loop servo controlled system of the loading profile (eg. 2/3<sup>rd</sup> part as a ramp with parabolic waveform at each end). The resulting error signal (difference between commanded and actual load) reduces until at the turning point it reduces to theoretically zero. In practice, the error signal reduces to a finite value due to valve balance offsets. To reduce this static loop offset (which could cause the null-pacer to malfunction), 'reset integration' was switched into the loop as the command signal reached a turning point and "dwelled" at the plateau. These switched integrators turned the control system from "proportional" to "proportional plus integral" at the excursion "dwells". Hence by effectively increasing the D.C. gain of the loop, the static loop offsets were cancelled. Thus all channels could be guaranteed to reach and signify a null. Once all channels were inside the null tolerance band, the computer received the "master null" flag and it then read the load reached by each channel. The values for the corresponding channel and turning point were compared with that stored in memory. If differences were detected, and the values were greater than those arbitrarily set for that channel and turning point, then a primary error signal was generated and the load cycling was paused. If the error signal exceeded a larger arbitrarily set limit, then a secondary error signal halted the control system.

During the excursion between turning points, the integrator was switched out of circuit and the tracking ability of the servo system was determined by both the allowable loop gains of each channel, and the slew rate (cycling speed). The allowable maximum slew rate for each jack was programmed into the computer. The excursion time (common for all jacks) for each load cycle was selected by taking the maximum time that any particular jack could perform the excursion and setting that time as the common base time for all jacks.

There were also many fail-safe devices incorporated in the system. The fail-safe sequence was initiated when a fault occurred which in turn operated a fast acting servo valve isolator (3 to 4 milliseconds) that isolated every servo-valve coil and was followed 40-60 milliseconds later by solenoid operated hydraulic control valves. This action deactivated the load system until the fault was cleared or the specimen was safely unloaded.

The servo-valve and solenoid operated control valves were installed in a unit called the "valve pack". One valve pack per channel was situated in close proximity to its own jack.

The control console contained the pressure gauges for various systems, emergency stop button, manually operated single channel unload buttons and hydraulic stop valves for the system. The instrumentation controlled the progressive levels of readiness that the system reached before it was prudent for the computer to start the

flight-by-flight loading program. The hydraulic stop valves cut off pressure to the valve packs upon a fault sequence being initiated. The console was located adjacent to the test rig and permitted the operator to manually over-ride the system in cases of emergency.

### **Commissioning of Test Rig**

The commissioning phase started with preliminary testing of all the electro-hydraulic closed loop servo controlled load channels in the two specially designed acceptance test rigs before being installed on the wing loading rig.

In these acceptance test rigs, each complete system loop, comprising of an actuator, double bridge load cell, valve pack and servo-amplifier was tested for correct operation and then calibrated and tuned for tracking, offsets etc. An important test during the tuning procedure was the square wave test, which measured the response of the loading channel. Restrictors were also adjusted in dump valves within the valve packs so that all jacks would unload smoothly at the same rate from the fail-safe lock-up. The computer command and monitor system was tested on these individual channels in the acceptance test rigs.

On completion of this initial tuning test, the load channel was installed in the wing loading rig and connected to the computer. When all channels were installed, preliminary command signals from the computer (using paper punched tape input), were given to each load channel working at levels of low-pressure oil and controlled through the control console.

As confidence increased, all channels were signalled to apply a very small load while one channel at a time was given a further square wave test to set the loop gains and lag filter time constants to optimise that channel's time response. This was iteratively done for all channels resulting in an acceptable and stable response for the whole system.

Upon completion, a series of calibration runs were made to check the validity of the test rig loading system. The wing had distributed loads applied that were representative of well defined flight cases for which strain data was available. Comparisons were made to provide the first check on how well flight conditions were being represented by the rig in the laboratory, and increased assurance in the ability of the control system to function as per design specifications. For those tests, the computer was programmed to apply the calibration case in steps of 10% full load.

There was good agreement with flight data for those gauges in identical position along the inboard section of the main spar and neighbouring skin areas. All eighty station strain records (Figure 8) were used for these calibration cases.

The time taken by the computer for all channels to reach null during "dwells" was a figure regarded as important (typically 200-300 milli-seconds). The slowest channels to

reach null (ie the effective pacing channels) were identified and “tweaked” to try to improve their response. This was most critical to the cycling rate.

Gradually, as each aspect of this complex control system was checked, an increase in the “slew” rate table of the jacks in the computer resulted in an increase in the cycling rate. Three factors influenced the system optimum running efficiency:

- i. width of the null bank; typically +/- 1.5% full-scale;
- ii. primary limit tolerance band, typically +/- 2% full-scale; and
- iii. slew rate.

Opening the width of the null band, shortened the time the computer spent at each turning point for all channels to reach the “master null” condition. Similarly, increasing the width of the primary limit tolerance reduced the number of times the control system paused while the operator investigated the cause.

## Appendix D: Summary of Conclusions from the Mirage Scatter Factor for Wing Fatigue Test Meeting

Present: F.G. Blight (Chairman), Dr F.H. Hooke, Dr. A.O. Payne, Dr. D.G. Ford, Dr. G.S. Jost.

Date: 5-7-1974

1. By whatever method the scatter factor is derived, there is intrinsic uncertainty about the true probability of failure if the population mean and/or variances are based upon small samples. The smaller the sample the greater the uncertainty.
2. If the acceptable probability of failure (POF) is 0.1%, then the safe life is bounded by the 0.1% tail of the population distribution, ie. by the 0.1 percentile of the population. The uncertainty that arises from "sampling" (ie. basing calculations on small samples), may be grasped by calculating "confidence intervals" for the 0.1 percentile. Calculations can also be made using confidence intervals which allow for uncertainty in the population mean value through estimating on a sample of only one test result, and also uncertainty in the variance arising from estimating on the test series in this case, of approximately 124 test results<sup>4</sup>.
3. Uncertainty arising from small test series can be allowed for by one of the two methods:-
  - (i) The method of "Atkinson", in which the population 0.1 percentile is estimated using the lower (say 95% or 99%) confidence limit for the population mean value and/or the upper (say 95% or 99%) confidence limit for the population variance value.
  - (ii) The "Kloos and Turner" method, in which the safe life is a bound and located at a certain deviation from the sample mean. Such a member of the population (drawn at random), will fall below that bound with an average or "expected value" of the probability of failure equal to the acceptable value. For a normally distributed variate, and  $N[F]$  (or POF) = 0.001, the deviation is  $-3.09\delta\sqrt{1+1/n}$  ( $n$  being the number of members in the sample for determining mean and  $\delta$  = standard deviation). This method has been used for many years at ARL, and it was agreed to be appropriate in this case.
4. The multiplying factor  $\sqrt{1+1/n}$  may be regarded as a multiplier to the spread of the population, arising from estimating the population mean using a small sample. It thus provides an answer to the question "what confidence can be placed in a single test result?"

---

<sup>4</sup> The editors could not trace the source of these results.

5. Where variance is not known precisely but is estimated from non-infinite sample of say ' $n$ ' specimens, the deviate in paragraph (3) is distributed not normally, but as student's " $t$ " with a number of degrees of freedom which is related to  $n$ : In this case of  $n = 124$ . The difference in the scatter factor is small.
6. It was generally agreed that in the case of the Mirage wing test, the use of the Kloos and Turner method, and the factor  $\sqrt{1+1/n}$  was appropriate.
7. The Mirage wing test had an asymmetric spectrum; for aluminium alloy structures under such spectra the pooled value of  $\delta$  (strictly  $n$ ) is 0.089. Using this figure the scatter factor (S.F.) is about 2.6; Drs. Hooke and Ford favoured the use of this value.
8. Dr Jost made two points concerning the applicability of the above value of standard deviation to the present situation. First it derives from fatigue test data on aircraft structures which are, typically, 20 to 30 years old. The Mirage is of a later era in detail, fatigue design and manufacturing quality. Secondly, although there is much evidence to suggest that smaller scatter is associated with asymmetric spectra than otherwise, the spectrum characteristic responsible for influencing scatter is still unknown.

Reasons were given supporting the adoption of a variance based on pooling of results for asymmetric spectra with symmetric spectra. Both Drs Payne and Jost favoured some increase in the adopted value of standard deviation to allow for the above uncertainties in the calculation of the scatter factor.

9. Dr Payne, in his paper (Ref. 61) had increased this value of standard deviation to the upper 99% confidence level, viz. 0.11, for reasons of conservatism, because of his uncertainty that the pooled variance for all aluminium alloy structures under asymmetric spectra adequately represents Mirage wings. This resulted in a scatter factor of 3.25.
10. Assuming that the standard deviation of 0.089 for aluminium alloy structures under asymmetric spectra is applicable, a scatter factor of 3.25 would give an expected value of probability of failure much lower than 0.001; nearer 0.00005. On the other hand, the assumption that the standard deviation of 0.11 is applicable, together with the adoption of a scatter factor of 3.25 would lead to a value of probability of failure of about 0.001.
11. For the purpose of defining ARL's view to be put forward to Air Commodore Cuming and Air Commodore Noble at their visit to ARL on the 9<sup>th</sup> July 1974, it was proposed (by the Chief Superintendent F.G. Blight and generally agreed), that the figure of 3.25 should stand as an upper limit to the value of scatter factor which ARL considered necessary. No decision was made on the question that ARL should recommend to the RAAF the figure 3.25 or the figure 2.6 or any other figure.

12. It is the RAAF's responsibility to decide whether to adopt the 0.089 figure or to increase it to allow for unknowns.

13. Structures Division will produce a graph (Figure 37) of scatter factor versus standard deviation (on the assumptions that) the:

- (a) population mean is determined on one test; and
- (b) variance is known exactly so that students t distribution is not needed.

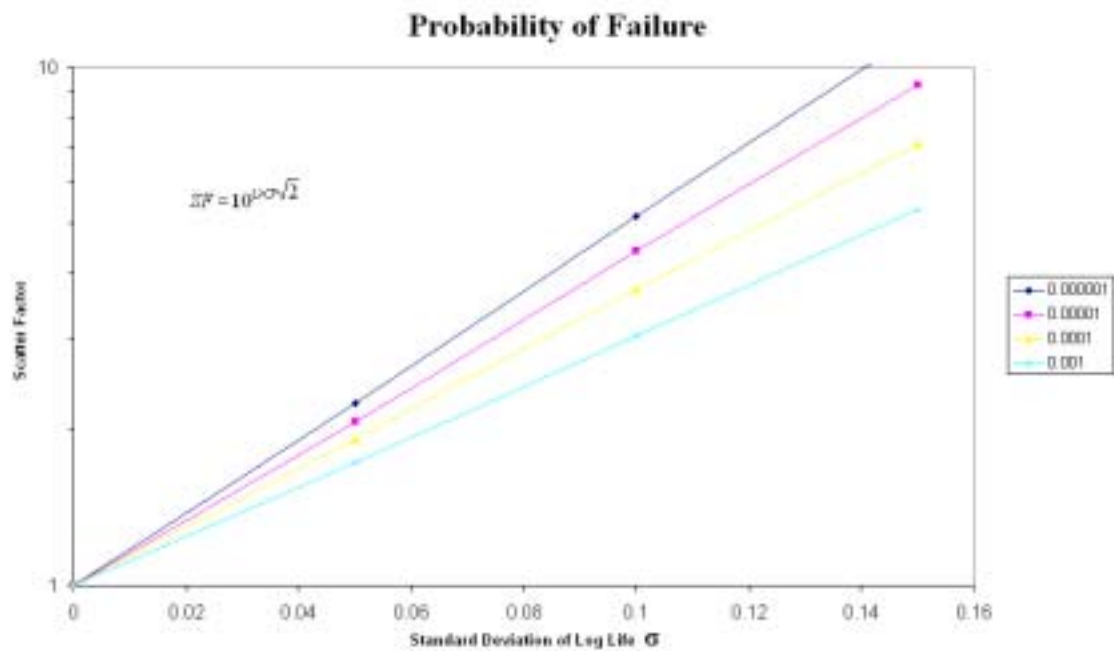


Figure 37: Scatter Factors versus Probability of Failure

DEFENCE SCIENCE AND TECHNOLOGY ORGANISATION DOCUMENT CONTROL DATA				1. PRIVACY MARKING/CAVEAT (OF DOCUMENT)	
2. TITLE  A Record of the Australian Mirage Wing Fatigue Test			3. SECURITY CLASSIFICATION (FOR UNCLASSIFIED REPORTS THAT ARE LIMITED RELEASE USE (L) NEXT TO DOCUMENT CLASSIFICATION)  Document (U) Title (U) Abstract (U)		
4. AUTHOR(S) -edited by  R. Krieser and L. Molent			5. CORPORATE AUTHOR  Platforms Sciences Laboratory 506 Lorimer St Fishermans Bend Victoria 3207 Australia		
6a. DSTO NUMBER DSTO-TR-1561		6b. AR NUMBER AR-013-047		6c. TYPE OF REPORT Technical Report	7. DOCUMENT DATE March 2004
8. FILE NUMBER 2004/1004202		9. TASK NUMBER 01/143	10. TASK SPONSOR DGTA	11. NO. OF PAGES 71	12. NO. OF REFERENCES 61
13. URL on the World Wide Web  <a href="http://www.dsto.defence.gov.au/corporate/reports/DSTO-TR-1561.pdf">http://www.dsto.defence.gov.au/corporate/reports/DSTO-TR-1561.pdf</a>				14. RELEASE AUTHORITY  Chief, Air Vehicles Division	
15. SECONDARY RELEASE STATEMENT OF THIS DOCUMENT  <i>Approved for public release</i>  <small>OVERSEAS ENQUIRIES OUTSIDE STATED LIMITATIONS SHOULD BE REFERRED THROUGH DOCUMENT EXCHANGE, PO BOX 1500, EDINBURGH, SA 5111</small>					
16. DELIBERATE ANNOUNCEMENT  No Limitations					
17. CITATION IN OTHER DOCUMENTS <span style="float: right;">Yes</span>					
18. DEFTEST DESCRIPTORS  Military aircraft, Mirage III aircraft, strain measurements, aircraft fatigue data analysis systems, aircraft fatigue, life (durability), aircraft structures, fatigue life, fatigue tests.					
19. ABSTRACT A full-scale fatigue test was completed in August 1974 on a Mirage III0 starboard wing utilising a loading spectrum as specified by the Royal Australian Air Force (RAAF). To satisfy a variety of RAAF missions, twelve (12) servo-hydraulic actuators situated at critical locations on the wing reproduced the measured flight strains. The fatigue loading flight-by-flight sequence was derived from fatigue meter data that was obtained from the Mirage fleet and from continuous records from an instrumented Mirage in the squadron service. The conduct and results of this innovative test are summarised here.					